Inverse electromagnetic diffraction by biperiodic dielectric gratings

2017 Inverse Problems 33 085004

(http://iopscience.iop.org/0266-5611/33/8/085004)

IOP Publishing Inverse Problems

Inverse Problems **33** (2017) 085004 (29pp) https://doi.org/10.1088/1361-6420/aa76b9

Inverse electromagnetic diffraction by biperiodic dielectric gratings

Xue Jiang[1] **and Peijun Li**[2,3]

[1] School of Science, Beijing University of Posts and Telecommunications Beijing 100876, People's Republic of China
[2] Department of Mathematics, Purdue University, West Lafayette, IN 47907, United States of America

E-mail: jxue@lsec.cc.ac.cn and lipeijun@math.purdue.edu

Received 12 December 2016, revised 10 May 2017
Accepted for publication 2 June 2017
Published 19 June 2017

Abstract

Consider the incidence of a time-harmonic electromagnetic plane wave onto a biperiodic dielectric grating, where the surface is assumed to be a small and smooth perturbation of a plane. The diffraction is modeled as a transmission problem for Maxwell's equations in three dimensions. This paper concerns the inverse diffraction problem which is to reconstruct the grating surface from either the diffracted field or the transmitted field. A novel approach is developed to solve the challenging nonlinear and ill-posed inverse problem. The method requires only a single incident field and is realized via the fast Fourier transform. Numerical results show that it is simple, fast, and stable to reconstruct biperiodic dielectric grating surfaces with super-resolved resolution.

Keywords: Maxwell's equations, inverse diffraction, near-field imaging, biperiodic gratings

(Some figures may appear in colour only in the online journal)

1. Introduction

Consider the diffraction of a time-harmonic electromagnetic plane incident wave by a biperiodic structure, which is called a crossed or two-dimensional grating in optical community. Given the structure and the incident field, the direct problem is to determine the diffracted field. The inverse problem is to reconstruct the grating surface from measured field. This paper concerns the latter. Diffractive gratings have been widely used in micro-optics including the design and fabrication of optical elements such as corrective lenses, anti-reflective interfaces, beam splitters, and sensors. Driven by the industrial applications, the diffraction grating

[3] Author to whom any correspondence should be addressed.

problems have received ever-lasting attention in the engineering and applied mathematical communities [14, 48]. An introduction to this topic can be found in the monograph [50]. We refer to [12] for a comprehensive review on the mathematical modeling and computational methods for these problems.

The inverse diffraction problems have been studied extensively for one-dimensional gratings, where the structures are invariant in one direction and the model of Maxwell's equations can be simplified into the Helmholtz equation. Mathematical results, such as uniqueness and stability, are established by many researchers [10, 15, 25, 39, 43]. Computationally, a number of methods are developed [9, 21, 22, 26, 36, 38, 42]. Numerical solutions can be found in [8, 31, 34, 44] for solving general inverse surface scattering problems. There are also many work done for two-dimensional gratings, where Maxwell's equations must be considered. We refer to [3, 11, 20, 35, 45] for the existence, uniqueness, and numerical approximations of solutions for the direct problems. Mathematical studies on uniqueness can be found in [2, 23, 24, 40, 41, 52] for the inverse problems. Numerical results are very rare for the inverse problems due to the nonlinearity, ill-posedness, and large scale computation [46]. Despite a great number of work done for the inverse diffraction problems, they addressed the classical inverse scattering problems. The reconstructed resolution was limited by Rayleigh's criterion, approximately half of the incident wavelength, also known as the diffraction limit [32].

When a light beam illuminates a sample characterized by a fine structure (with details smaller than one half the wavelength), it will be converted into propagating components, which are able to propagate towards the remote (far-field) detector, and evanescent components, which are confined on the surface. The first ones are associated to the low spatial frequencies of the object whereas the second ones are connected to their high frequencies, which do not obey the Rayleigh criterion and contribute to the subwavelength (a small fraction of the wavelength) resolution. Near-field imaging deals with phenomena involving evanescent waves which become significant when the sizes of the samples are of the order of the wavelength or smaller. By bringing a scanner into the near-field (subwavelength) of the sample, the high frequency evanescent field can be measured and thus images with subwavelength (super-resolved) resolution may be obtained [33, 37].

Recently, a novel approach has been developed to solve inverse surface scattering problems in various near-field imaging modalities [16–18, 30] including the inverse electromagnetic diffraction by a perfectly electrically conducting grating [13]. The work in [13] presents the first quantitative method for solving the inverse diffraction problem of Maxwell's equations with super-resolved resolution. As is known, the perfect electric conductor is an idealized material exhibiting infinite electrical conductivity and may not exist in nature. In this paper, we consider a realistic dielectric grating and the result is closer to practical applications. The more elaborate techniques differ from the existing work because a complicated transmission problem of Maxwell's equations needs to be studied. Related work on near-field imaging can be found in [19, 28, 29, 46]. We refer to [4, 5] for a related interface reconstruction problem and its stability and resolution estimates. As is known, it is impossible to achieve super-resolved imaging in the far field unless resonant or high contrast structures are used. The mathematical theory of super-resolution can be found in [6, 7] on these aspects.

Specifically, we consider the incidence of an electromagnetic plane wave on a dielectric crossed grating, where the surface is assumed to be a small and smooth deformation of a plane. The diffraction is modeled as a transmission problem for Maxwell's equations in three dimensions. The method begins with the transformed field expansion and reduces the boundary value problem into a successive sequence of two-point boundary value problems. Dropping higher order terms in the expansion, we linearize the nonlinear inverse problem and obtain explicit reconstruction formulas for both the reflection and transmission configurations.

A spectral cut-off regularization is adopted to suppress the exponential growth of the noise in the evanescent wave components, which carry high spatial frequency of the surface and contribute to the super resolution. The method requires only a single illumination with one polarization, one frequency, and one incident direction, and is realized via the fast Fourier transform. The numerical results are computed by using synthetic scattering data provided by an adaptive edge element method with a perfectly matched absorbing layer [20]. Three numerical examples, one smooth surface and two non-smooth surfaces, are presented to demonstrate the effectiveness of the proposed method. Careful numerical studies are carried for the influence of all the parameters on the reconstructions. The results show that the method is simple, fast, and stable to reconstruct dielectric crossed grating surfaces with subwavelength resolution.

The paper is organized as follows. In section 2, the model problem is introduced. Section 3 presents the transformed field expansion to obtain the analytic solution of the direct problem. Explicit reconstruction formulas are derived for the inverse problem in section 4. Numerical examples are reported in section 5. The paper is concluded with some general remarks and direction for future work in section 6.

2. Model problem

In this section, we define some notation and introduce a boundary value problem for the diffraction by a biperiodic dielectric grating.

2.1. Maxwell's equations

Let us first specify the problem geometry. Denote $(\rho, z) \in \mathbb{R}^3$, where $\rho = (x, y) \in \mathbb{R}^2$. As seen in figure 1, the problem may be restricted to a single period of $\Lambda = (\Lambda_1, \Lambda_2)$ in ρ due to the periodicity of the structure. Let the surface in one period be described by $S = \{(\rho, z) \in \mathbb{R}^3 : z = \phi(\rho),\ 0 < x < \Lambda_1, 0 < y < \Lambda_2\}$, where $\phi \in C^2(\mathbb{R}^2)$ is a biperiodic grating surface function. We assume that

$$\phi(\rho) = \delta\psi(\rho), \tag{2.1}$$

where $\delta > 0$ is a small surface deformation parameter, $\psi \in C^2(\mathbb{R}^2)$ is also a biperiodic function and describes the shape of the grating surface.

We let S be embedded in the rectangular slab:

$$\Omega = \{(\rho, z) \in \mathbb{R}^3 : z_- < z < z_+\} = \mathbb{R}^2 \times (z_-, z_+),$$

where $z_+ > 0$ and $z_- < 0$ are two constants. Hence the domain Ω is bounded by two plane surfaces $\Gamma_\pm = \{(\rho, z) \in \mathbb{R}^3 : z = z_\pm\}$. Let $\Omega_S^+ = \{(\rho, z) : z > \phi(\rho)\}$ and $\Omega_S^- = \{(\rho, z) : z < \phi(\rho)\}$ be filled with homogeneous materials which are characterized by the electric permittivity ε_+ and ε_-, respectively.

Let $(\mathbf{E}^{\text{inc}}, \mathbf{H}^{\text{inc}})$ be the incoming electromagnetc plane waves, where

$$\mathbf{E}^{\text{inc}} = \mathbf{p}e^{i\kappa_+(\alpha\cdot\rho-\beta z)}, \quad \mathbf{H}^{\text{inc}} = \left(\frac{\varepsilon_+}{\mu}\right)^{1/2} \mathbf{q}e^{i\kappa_+(\alpha\cdot\rho-\beta z)}. \tag{2.2}$$

Here $\kappa_+ = \omega(\mu\varepsilon_+)^{1/2}$ is the wavenumber in Ω_S^+, $\omega > 0$ is the angular frequency, μ is the magnetic permeability and is assumed to be a positive constant everywhere, $\alpha = (\alpha_1, \alpha_2)$, $\alpha_1 = \sin\theta_1 \cos\theta_2$, $\alpha_2 = \sin\theta_1 \sin\theta_2$, and $\beta = \cos\theta_1$, where θ_1 and θ_2 are the latitudinal and

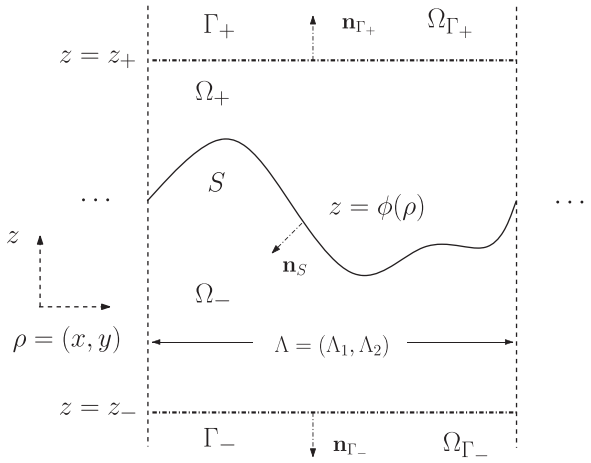

Figure 1. The problem geometry of a biperiodic dielectric grating.

longitudinal incident angles, respectively, which satisfy $0 \leqslant \theta_1 < \pi/2, 0 \leqslant \theta_2 < 2\pi$. Denote by $\mathbf{d} = (\alpha_1, \alpha_2, -\beta)$ the unit propagation direction vector. The unit polarization vectors $\mathbf{p} = (p_1, p_2, p_3)$ and $\mathbf{q} = (q_1, q_2, q_3)$ satisfy

$$\mathbf{p} \cdot \mathbf{d} = 0, \quad \mathbf{q} = \mathbf{d} \times \mathbf{p},$$

which gives explicitly that

$$q_1 = \alpha_2 p_3 + \beta p_2, \quad q_2 = -(\alpha_1 p_3 + \beta p_1), \quad q_3 = \alpha_1 p_2 - \alpha_2 p_1.$$

For normal incident, i.e. $\theta_1 = 0$, we have

$$\alpha_1 = 0, \quad \alpha_2 = 0, \quad \beta = 1, \quad q_1 = p_2, \quad q_2 = -p_1, \quad q_3 = 0.$$

Hence we get from $|\mathbf{p}| = |\mathbf{q}| = 1$ that

$$p_1^2 + p_2^2 = 1, \quad p_3 = 0.$$

For simplicity, we focus on the normal incidence from now on since our method requires only a single incidence. In fact, this is the most convenient way to illuminate the grating structure. The method also works for non-normal incidence with obvious modifications.

Let $\mathbf{E}^{\text{inc}} = (E_1^{\text{inc}}, E_2^{\text{inc}}, E_3^{\text{inc}})$ and $\mathbf{H}^{\text{inc}} = (H_1^{\text{inc}}, H_2^{\text{inc}}, H_3^{\text{inc}})$. Under the normal incidence, the incoming plane waves (2.2) reduce to

$$E_j^{\text{inc}} = p_j \mathrm{e}^{-\mathrm{i}\kappa_+ z}, \quad H_j^{\text{inc}} = \left(\frac{\varepsilon_+}{\mu}\right)^{1/2} q_j \mathrm{e}^{-\mathrm{i}\kappa_+ z}, \tag{2.3}$$

which satisfy the time-harmonic Maxwell equation:

$$\nabla \times \mathbf{E}^{\text{inc}} - \mathrm{i}\omega\mu \mathbf{H}^{\text{inc}} = 0, \quad \nabla \times \mathbf{H}^{\text{inc}} + \mathrm{i}\omega\varepsilon_+ \mathbf{E}^{\text{inc}} = 0 \quad \text{in } \Omega_S^+.$$

The time-harmonic electromagnetic waves satisfy Maxwell's equations:

$$\nabla \times \mathbf{E} - \mathrm{i}\omega\mu \mathbf{H} = 0, \quad \nabla \times \mathbf{H} + \mathrm{i}\omega\varepsilon \mathbf{E} = 0 \quad \text{in } \mathbb{R}^3, \tag{2.4}$$

where $(\mathbf{E}, \mathbf{H})$ are the total electric and magnetic fields, and the dielectric permittivity

$$\varepsilon = \begin{cases} \varepsilon_+ & \text{in} \quad \Omega_S^+, \\ \varepsilon_- & \text{in} \quad \Omega_S^-. \end{cases}$$

Motivated by uniqueness, we are interested in periodic solutions of $(\mathbf{E}, \mathbf{H})$ in ρ with period Λ, i.e. $(\mathbf{E}, \mathbf{H})$ satisfy

$$\mathbf{E}(\rho + \Lambda, z) = \mathbf{E}(\rho, z), \quad \mathbf{H}(\rho + \Lambda, z) = \mathbf{H}(\rho, z).$$

The total fields can be decomposed into

$$(\mathbf{E},\, \mathbf{H}) = \begin{cases} (\mathbf{E}^{\text{inc}},\, \mathbf{H}^{\text{inc}}) + (\mathbf{E}^{\text{d}},\, \mathbf{H}^{\text{d}}) & \text{in} \quad \Omega_S^+, \\ (\mathbf{E}^{\text{t}},\, \mathbf{H}^{\text{t}}) & \text{in} \quad \Omega_S^-, \end{cases}$$

where $(\mathbf{E}^{\text{d}},\, \mathbf{H}^{\text{d}})$ are the diffracted fields and $(\mathbf{E}^{\text{t}},\, \mathbf{H}^{\text{t}})$ are the transmitted fields. They are required to satisfy the bounded outgoing wave condition.

2.2. Transparent boundary condition

In this section, we introduce transparent boundary conditions on $\Gamma_\pm$ which are equivalent to the bounded outgoing wave condition. The detailed derivation can be found in [21].

Let $n = (n_1,\, n_2) \in \mathbb{Z}^2$ and denote $\alpha_n = (\alpha_{1n},\, \alpha_{2n})$, where $\alpha_{1n} = 2\pi n_1/\Lambda_1$ and $\alpha_{2n} = 2\pi n_2/\Lambda_2$. For any vector field $\mathbf{u} = (u_1,\, u_2,\, u_3)$, denote its tangential components on $\Gamma_\pm$ by

$$\mathbf{u}_{\Gamma_\pm} = \mathbf{n}_{\Gamma_\pm} \times (\mathbf{u} \times \mathbf{n}_{\Gamma_\pm}) = (u_1(\rho, z_\pm),\, u_2(\rho, z_\pm),\, 0),$$

and its tangential traces on $\Gamma_\pm$ by

$$\begin{aligned} \mathbf{u} \times \mathbf{n}_{\Gamma_+} &= (u_2(\rho, z_+),\, -u_1(\rho, z_+),\, 0), \\ \mathbf{u} \times \mathbf{n}_{\Gamma_-} &= (-u_2(\rho, z_-),\, u_1(\rho, z_-),\, 0), \end{aligned}$$

where $\mathbf{n}_{\Gamma_\pm} = (0,\, 0,\, \pm 1)$ are the unit normal vectors on $\Gamma_\pm$.

For any tangential vector $\mathbf{u}(\rho, z_+) = (u_1(\rho, z_+),\, u_2(\rho, z_+),\, 0)$ on Γ_+, where u_j are biperiodic functions in ρ with period Λ, we define the capacity operator T_+:

$$T_+\mathbf{u} = (v_1(\rho, z_+),\, v_2(\rho, z_+),\, 0), \tag{2.5}$$

where v_j are also biperiodic functions in ρ with the same period Λ. Here u_j and v_j have the following Fourier series expansions

$$u_j(\rho, z_+) = \sum_{n \in \mathbb{Z}^2} u_{jn}(z_+) \mathrm{e}^{\mathrm{i}\alpha_n \cdot \rho}, \quad v_j(\rho, z_+) = \sum_{n \in \mathbb{Z}^2} v_{jn}(z_+) \mathrm{e}^{\mathrm{i}\alpha_n \cdot \rho},$$

and the Fourier coefficients u_{jn} and v_{jn} satisfy

$$\begin{cases} v_{1n}(z_+) = \frac{1}{\omega\mu\beta_n^+} \left[(\kappa_+^2 - \alpha_{2n}^2) u_{1n}(z_+) + \alpha_{1n}\alpha_{2n} u_{2n}(z_+)\right], \\ v_{2n}(z_+) = \frac{1}{\omega\mu\beta_n^+} \left[(\kappa_+^2 - \alpha_{1n}^2) u_{2n}(z_+) + \alpha_{1n}\alpha_{2n} u_{1n}(z_+)\right], \end{cases}$$

where

$$(\beta_n^+)^2 = \kappa_+^2 - |\alpha_n|^2 \quad \text{with } \operatorname{Im} \beta_n^+ > 0. \tag{2.6}$$

We exclude possible resonance by assuming that $\beta_n^+ \neq 0$ for all $n \in \mathbb{Z}^2$.

Using the capacity operator (2.5), we impose a transparent boundary condition on Γ_+:

$$T_+(\mathbf{E}_{\Gamma_+} - \mathbf{E}_{\Gamma_+}^{\text{inc}}) = (\mathbf{H} - \mathbf{H}^{\text{inc}}) \times \mathbf{n}_{\Gamma_+},$$

which maps the tangential component of the scattered electric field to the tangential trace of the scattered magnetic field. Equivalently, the above boundary condition can be written as

$$(\nabla \times \mathbf{E}) \times \mathbf{n}_{\Gamma_+} = \mathrm{i}\omega\mu T_+ \mathbf{E}_{\Gamma_+} + \mathbf{f}, \tag{2.7}$$

where

$$\mathbf{f} = \mathrm{i}\omega\mu(\mathbf{H}^{\mathrm{inc}} \times \mathbf{n}_{\Gamma_+} - T_+ \mathbf{E}^{\mathrm{inc}}_{\Gamma_+}) = (f_1, f_2, f_3).$$

Recalling the incident fields (2.3) and using the boundary operator (2.5), we have explicitly that

$$f_j = -2\mathrm{i}\kappa_+ p_j \mathrm{e}^{-\mathrm{i}\kappa_+ z_+}.$$

Similarly, for any given tangential vector $\mathbf{u}(\rho, z_-) = (u_1(\rho, z_-), u_2(\rho, z_-), 0)$ on Γ_-, where $u_j(\rho, z_-)$ is a biperiodic function in ρ with period Λ, we define the capacity operator T_-:

$$T_- \mathbf{u} = (v_1(\rho, z_-), v_2(\rho, z_-), 0), \tag{2.8}$$

where v_j is also a biperiodic function in ρ with the same period Λ. Here u_j and v_j have the following Fourier series expansions

$$u_j(\rho, z_-) = \sum_{n\in\mathbb{Z}^2} u_{jn}(z_-)\mathrm{e}^{\mathrm{i}\alpha_n\cdot\rho}, \quad v_j(\rho, z_-) = \sum_{n\in\mathbb{Z}^2} v_{jn}(z_-)\mathrm{e}^{\mathrm{i}\alpha_n\cdot\rho},$$

and the Fourier coefficients u_{jn} and v_{jn} satisfy

$$\begin{cases} v_{1n}(z_-) = \frac{1}{\omega\mu\beta_n^-}\left[(\kappa_-^2 - \alpha_{2n}^2)u_{1n}(z_-) + \alpha_{1n}\alpha_{2n}u_{2n}(z_-)\right], \\ v_{2n}(z_-) = \frac{1}{\omega\mu\beta_n^-}\left[(\kappa_-^2 - \alpha_{1n}^2)u_{2n}(z_-) + \alpha_{1n}\alpha_{2n}u_{1n}(z_-)\right], \end{cases}$$

where $\kappa_- = \omega(\mu\varepsilon_-)^{1/2}$ is the wavenumber in Ω_S^- and

$$(\beta_n^-)^2 = \kappa_-^2 - |\alpha_n|^2 \quad \text{with } \mathrm{Im}\,\beta_n^- > 0. \tag{2.9}$$

Here we also assume that $\beta_n^- \neq 0$ for all $n \in \mathbb{Z}^2$.

Based on (2.8), a transparent boundary condition may be proposed on Γ_-:

$$T_- \mathbf{E}_{\Gamma_-} = \mathbf{H} \times \mathbf{n}_{\Gamma_-},$$

which is equivalent to

$$(\nabla \times \mathbf{E}) \times \mathbf{n}_{\Gamma_-} = \mathrm{i}\omega\mu T_- \mathbf{E}_{\Gamma_-}. \tag{2.10}$$

2.3. Transmission problem

Taking curl on both sides of (2.4), we may eliminate the magnetic field and obtain a decoupled equation for the electric field:

$$\nabla \times (\nabla \times \mathbf{E}) - \kappa^2 \mathbf{E} = 0 \quad \text{in } \Omega, \tag{2.11}$$

where the wavenumber

$$\kappa = \begin{cases} \kappa_+ & \text{in } \Omega_S^+, \\ \kappa_- & \text{in } \Omega_S^-. \end{cases}$$

Denote $\Omega_+ = \Omega_S^+ \cap \Omega = \{(\rho, z) : \phi(\rho) < z < z_+\}$ and $\Omega_- = \Omega_S^- \cap \Omega = \{(\rho, z) : z_- < z < \phi(\rho)\}$. Let $\mathbf{E}^+$ and $\mathbf{E}^-$ be the restriction of $\mathbf{E}$ in Ω_+ and Ω_-, respectively, i.e.

$\mathbf{E}^{\pm} = \mathbf{E}|_{\Omega_{\pm}}$. It is useful to have an equivalent scalar form of (2.11) when applying the transformed field expansion. Denote $\mathbf{E}^{\pm} = (E_1^{\pm}, E_2^{\pm}, E_3^{\pm})$. We may reformulate (2.11) into the Helmholtz equation:

$$\Delta E_j^{\pm} + \kappa_{\pm}^2 E_j^{\pm} = 0 \quad \text{in } \Omega_{\pm}. \tag{2.12}$$

The transparent boundary conditions (2.7) and (2.10) can be written as

$$\begin{cases} \partial_z E_1^+ - \partial_x E_3^+ = \mathrm{i}\omega\mu H_1^+ + f_1, \\ \partial_z E_2^+ - \partial_y E_3^+ = \mathrm{i}\omega\mu H_2^+ + f_2, \end{cases} \tag{2.13}$$

and

$$\begin{cases} \partial_z E_1^- - \partial_x E_3^- = -\mathrm{i}\omega\mu H_1^-, \\ \partial_z E_2^- - \partial_y E_3^- = -\mathrm{i}\omega\mu H_2^-, \end{cases} \tag{2.14}$$

where the Fourier coefficients of the periodic functions $H_1^{\pm}$ and $H_2^{\pm}$ are given by

$$\begin{cases} H_{1n}^{\pm}(z_{\pm}) = \frac{1}{\omega\mu\beta_n^{\pm}} \left[(\kappa_{\pm}^2 - \alpha_{2n}^2) E_{1n}^{\pm}(z_{\pm}) + \alpha_{1n}\alpha_{2n} E_{2n}^{\pm}(z_{\pm}) \right], \\ H_{2n}^{\pm}(z_{\pm}) = \frac{1}{\omega\mu\beta_n^{\pm}} \left[(\kappa_{\pm}^2 - \alpha_{1n}^2) E_{2n}^{\pm}(z_{\pm}) + \alpha_{1n}\alpha_{2n} E_{1n}^{\pm}(z_{\pm}) \right]. \end{cases}$$

Here $E_{1n}^{\pm}(z_{\pm})$ and $E_{2n}^{\pm}(z_{\pm})$ are the Fourier coefficients of the periodic electric field $E_1^{\pm}(\rho, z_{\pm})$ and $E_2^{\pm}(\rho, z_{\pm})$, respectively.

The continuity conditions are needed to reformulate the boundary value problem into a transmission problem. It is known that the tangential traces of the electric and magnetic fields are continuous across the grating surface, i.e.

$$\mathbf{E}^+ \times \mathbf{n}_S = \mathbf{E}^- \times \mathbf{n}_S, \quad \mathbf{H}^+ \times \mathbf{n}_S = \mathbf{H}^- \times \mathbf{n}_S, \quad z = \phi(\rho),$$

where $\mathbf{n}_S = (\phi_x, \phi_y, -1)$ is the normal vector on S pointing from Ω_S^+ to Ω_S^-. Explicitly, we have the continuity conditions

$$\begin{cases} E_2^+ + \phi_y E_3^+ = E_2^- + \phi_y E_3^-, \\ E_1^+ + \phi_x E_3^+ = E_1^- + \phi_x E_3^-, \end{cases} \tag{2.15}$$

and

$$\begin{cases} \left(\partial_z E_1^+ - \partial_x E_3^+\right) + \phi_y \left(\partial_x E_2^+ - \partial_y E_1^+\right) \\ \qquad = (\partial_z E_1^- - \partial_x E_3^-) + \phi_y (\partial_x E_2^- - \partial_y E_1^-), \\ \left(\partial_y E_3^+ - \partial_z E_2^+\right) + \phi_x \left(\partial_x E_2^+ - \partial_y E_1^+\right) \\ \qquad = \left(\partial_y E_3^- - \partial_z E_2^-\right) + \phi_x \left(\partial_x E_2^- - \partial_y E_1^-\right). \end{cases} \tag{2.16}$$

The transparent boundary conditions (2.13) and (2.14) and the continuity conditions (2.15) and (2.16) are not enough to determine the fields $\mathbf{E}_j^{\pm}$. Additional information can be obtained from the divergence free conditions

$$\partial_x E_1^{\pm} + \partial_y E_2^{\pm} + \partial_z E_3^{\pm} = 0 \quad \text{in } \Omega_{\pm}. \tag{2.17}$$

Given the grating surface function $\phi(\rho)$, the direct problem is to determine the fields $\mathbf{E}_j^{\pm}$. This work is focused on the inverse problem, which is to reconstruct the grating surface function $\phi(\rho)$ from the tangential traces of the total field measured at either Γ_+, i.e. $\mathbf{E}(\rho, z_+) \times \mathbf{n}_{\Gamma_+} = (E_1(\rho, z_+), E_2(\rho, z_+), 0)$ called the reflection configuration, or Γ_-, i.e.

$\mathbf{E}(\rho, z_-) \times \mathbf{n}_{\Gamma_-} = (-E_1(\rho, z_-), E_2(\rho, z_-), 0)$ called the transmission configuration. In particular, we are interested in the inverse problem in near-field regime where the measurement distance $|z_\pm|$ is much smaller than the wavelength $\lambda = 2\pi/\kappa_+$ of the incident field.

3. Transformed field expansion

In this section, we introduce the transformed field expansion to analytically derive the solution for the direct problem. We refer to [27, 47, 49] for solving the direct and inverse surface scattering problems by using the transformed field expansion and related boundary perturbation method.

3.1. Change of variables

Consider the change of variables:

$$\tilde{x} = x, \quad \tilde{y} = y, \quad \tilde{z} = z_+ \left(\frac{z - \phi}{z_+ - \phi} \right), \quad \phi < z < z_+,$$

and

$$\tilde{x} = x, \quad \tilde{y} = y, \quad \tilde{z} = z_- \left(\frac{z - \phi}{z_- - \phi} \right), \quad z_- < z < \phi,$$

which maps the domain Ω_+ and Ω_- into rectangular slabs $D_+ = \{(\tilde{\rho}, \tilde{z}) \in \mathbb{R}^3 : 0 < \tilde{z} < z_+\}$ and $D_- = \{(\tilde{\rho}, \tilde{z}) \in \mathbb{R}^3 : z_- < z < 0\}$, respectively.

We seek to restate the diffractive grating problem in the new coordinate. Introduce a new function $\tilde{\mathbf{E}}^\pm = (\tilde{E}_1^\pm, \tilde{E}_2^\pm, \tilde{E}_3^\pm)$ and let $\tilde{E}_j^\pm(\tilde{x}, \tilde{y}, \tilde{z}) = E_j^\pm(x, y, z)$ under the transformation. After tedious but straightforward calculations, it can be verified from (2.12) that the total electric field, upon dropping the tilde, satisfies the equation

$$\begin{aligned} & c_1^\pm \frac{\partial^2 E_j^\pm}{\partial x^2} + c_1^\pm \frac{\partial^2 E_j^\pm}{\partial y^2} + c_2^\pm \frac{\partial^2 E_j^\pm}{\partial z^2} - c_3^\pm \frac{\partial^2 E_j^\pm}{\partial x \partial z} \\ & \qquad - c_4^\pm \frac{\partial^2 E_j^\pm}{\partial y \partial z} - c_5^\pm \frac{\partial E_j^\pm}{\partial z} + \kappa_\pm^2 c_1^\pm E_j^\pm = 0 \quad \text{in } D_\pm, \end{aligned} \tag{3.1}$$

where

$$\begin{aligned} c_1^\pm &= (z_\pm - \phi)^2, \\ c_2^\pm &= (\phi_x^2 + \phi_y^2)(z_\pm - z)^2 + z_\pm^2, \\ c_3^\pm &= 2\phi_x (z_\pm - z)(z_\pm - \phi), \\ c_4^\pm &= 2\phi_y (z_\pm - z)(z_\pm - \phi), \\ c_5^\pm &= (z_\pm - z)\big[(\phi_{xx} + \phi_{yy})(z_\pm - \phi) + 2(\phi_x^2 + \phi_y^2)\big]. \end{aligned}$$

The transparent boundary conditions (2.13) and (2.14) reduce to

$$\begin{cases} \left(\frac{z_+}{z_+ - \phi} \right) \partial_z E_1^+ - \partial_x E_3^+ = \mathrm{i}\omega\mu H_1^+ + f_1, \\ \left(\frac{z_+}{z_+ - \phi} \right) \partial_z E_2^+ - \partial_y E_3^+ = \mathrm{i}\omega\mu H_2^+ + f_2, \end{cases} \tag{3.2}$$

and

$$\begin{cases} \left(\frac{z_-}{z_- - \phi}\right) \partial_z E_1^- - \partial_x E_3^- = -\mathrm{i}\omega\mu H_1^-, \\ \left(\frac{z_-}{z_- - \phi}\right) \partial_z E_2^- - \partial_y E_3^- = -\mathrm{i}\omega\mu H_2^-. \end{cases} \tag{3.3}$$

The continuity conditions (2.15) and (2.16) are changed to

$$\begin{cases} E_2^+ + \phi_y E_3^+ = E_2^- + \phi_y E_3^-, \\ E_1^+ + \phi_x E_3^+ = E_1^- + \phi_x E_3^-, \end{cases} \tag{3.4}$$

and

$$\begin{cases} \left(\frac{z_+}{z_+ - \phi}\right) \left[\phi_x \partial_z E_3^+ - \phi_x \phi_y \partial_z E_2^+ + (1+\phi_y^2)\partial_z E_1^+\right] \\ \qquad - \left(\partial_x E_3^+ - \phi_y \partial_x E_2^+ + \phi_y \partial_y E_1^+\right) \\ = \left(\frac{z_-}{z_- - \phi}\right) \left[\phi_x \partial_z E_3^- - \phi_x \phi_y \partial_z E_2^- + (1+\phi_y^2)\partial_z E_1^-\right] \\ \qquad - \left(\partial_x E_3^- - \phi_y \partial_x E_2^- + \phi_y \partial_y E_1^-\right), \\ \left(\frac{z_+}{z_+ - \phi}\right) \left[\phi_y \partial_z E_3^+ + (1+\phi_x^2)\partial_z E_2^+ - \phi_x \phi_y \partial_z E_1^+\right] \\ \qquad - \left(\partial_y E_3^+ + \phi_x \partial_x E_2^+ - \phi_x \partial_y E_1^+\right) \\ = \left(\frac{z_-}{z_- - \phi}\right) \left[\phi_y \partial_z E_3^- + (1+\phi_x^2)\partial_z E_2^- - \phi_x \phi_y \partial_z E_1^-\right] \\ \qquad - \left(\partial_y E_3^- + \phi_x \partial_x E_2^- - \phi_x \partial_y E_1^-\right). \end{cases} \tag{3.5}$$

The divergence free condition (2.17) becomes

$$\begin{aligned} \partial_x E_1^\pm + \partial_y E_2^\pm - \left(\frac{z_\pm - z}{z_\pm - \phi}\right) (\phi_x \partial_z E_1^\pm + \phi_y \partial_z E_2^\pm) \\ + \left(\frac{z_\pm}{z_\pm - \phi}\right) \partial_z E_3^\pm = 0 \quad \text{in } D_\pm. \end{aligned} \tag{3.6}$$

3.2. Power series

Recalling $\phi = \delta\psi$ in (2.1), we use a classical boundary perturbation argument and consider a formal expansion of $E_j^\pm$ in a power series of δ:

$$E_j^\pm(\rho, z; \delta) = \sum_{k=0}^{\infty} E_j^{\pm(k)}(\rho, z)\, \delta^k. \tag{3.7}$$

Substituting $\phi = \delta\psi$ and the power series expansion (3.7) into $c_j^\pm$ and (3.1), we may derive a recursion equation for $E_j^{\pm(k)}$:

$$\Delta E_j^{\pm(k)} + \kappa_\pm^2 E_j^{\pm(k)} = F_j^{\pm(k)} \quad \text{in } D_\pm, \tag{3.8}$$

where the nonhomogeneous term

$$
\begin{aligned}
F_j^{\pm(k)} =& \frac{2\psi}{z_\pm}\frac{\partial^2 E_j^{\pm(k-1)}}{\partial x^2} + \frac{2\psi}{z_\pm}\frac{\partial^2 E_j^{\pm(k-1)}}{\partial y^2} + \frac{2(z_\pm - z)\psi_x}{z_\pm}\frac{\partial^2 E_j^{\pm(k-1)}}{\partial x \partial z} \\
&+ \frac{2(z_\pm - z)\psi_y}{z_\pm}\frac{\partial^2 E_j^{\pm(k-1)}}{\partial y \partial z} + \frac{(z_\pm - z)(\psi_{xx} + \psi_{yy})}{z_\pm}\frac{\partial E_j^{\pm(k-1)}}{\partial z} + \frac{2\kappa_\pm^2 \psi}{z_\pm} E_j^{\pm(k-1)} \\
&- \frac{\psi^2}{z_\pm^2}\frac{\partial^2 E_j^{\pm(k-2)}}{\partial x^2} - \frac{\psi^2}{z_\pm^2}\frac{\partial^2 E_j^{\pm(k-2)}}{\partial y^2} - \frac{(z_\pm - z)^2(\psi_x^2 + \psi_y^2)}{z_\pm^2}\frac{\partial^2 E_j^{\pm(k-2)}}{\partial z^2} \\
&- \frac{2\psi\psi_x(z_\pm - z)}{z_\pm^2}\frac{\partial^2 E_j^{\pm(k-2)}}{\partial x \partial z} - \frac{2\psi\psi_y(z_\pm - z)}{z_\pm^2}\frac{\partial^2 E_j^{\pm(k-2)}}{\partial y \partial z} \\
&+ \frac{(z_\pm - z)\left[2(\psi_x^2 + \psi_y^2) - \psi(\psi_{xx} + \psi_{yy})\right]}{z_\pm^2}\frac{\partial E_j^{\pm(k-2)}}{\partial z} - \frac{\kappa_\pm^2 \psi^2}{z_\pm^2} E_j^{\pm(k-2)}.
\end{aligned}
$$

Here $\psi_x = \partial_x \psi(x, y)$ and $\psi_y = \partial_y \psi(x, y)$ are the partial derivatives.

Substituting (3.7) into the transparent boundary conditions (3.2) and (3.3), we obtain

$$
\begin{cases}
\partial_z E_1^{+(k)} - \partial_x E_3^{+(k)} = \mathrm{i}\omega\mu H_1^{+(k)} - f_1^{+(k)}, \\
\partial_z E_2^{+(k)} - \partial_y E_3^{+(k)} = \mathrm{i}\omega\mu H_2^{+(k)} - f_2^{+(k)},
\end{cases} \tag{3.9}
$$

and

$$
\begin{cases}
\partial_z E_1^{-(k)} - \partial_x E_3^{-(k)} = -\mathrm{i}\omega\mu H_1^{-(k)} - f_1^{-(k)}, \\
\partial_z E_2^{-(k)} - \partial_y E_3^{-(k)} = -\mathrm{i}\omega\mu H_2^{-(k)} - f_2^{-(k)},
\end{cases} \tag{3.10}
$$

where

$$
\begin{aligned}
&f_1^{+(0)} = -f_1,\ f_1^{+(1)} = \frac{\psi}{z_+}\partial_z E_1^{+(0)},\ f_1^{+(k)} = \frac{\psi}{z_+}\left(\partial_x E_3^{+(k-1)} + \mathrm{i}\omega\mu H_1^{+(k-1)}\right), \\
&f_2^{+(0)} = -f_2,\ f_2^{+(1)} = \frac{\psi}{z_+}\partial_z E_2^{+(1)},\ f_2^{+(k)} = \frac{\psi}{z_+}\left(\partial_y E_3^{+(k-1)} + \mathrm{i}\omega\mu H_2^{+(k-1)}\right),
\end{aligned}
$$

and

$$
\begin{aligned}
&f_1^{-(0)} = 0,\ f_1^{-(1)} = \frac{\psi}{z_-}\partial_z E_1^{-(0)},\ f_1^{-(k)} = \frac{\psi}{z_-}\left(\partial_x E_3^{-(k-1)} - \mathrm{i}\omega\mu H_1^{-(k-1)}\right), \\
&f_2^{-(0)} = 0,\ f_2^{-(1)} = \frac{\psi}{z_-}\partial_z E_2^{-(0)},\ f_2^{-(k)} = \frac{\psi}{z_-}\left(\partial_y E_3^{-(k-1)} - \mathrm{i}\omega\mu H_2^{-(k-1)}\right).
\end{aligned}
$$

Here the Fourier coefficients of $H_1^{\pm(k)}(\rho, z_\pm)$ and $H_2^{\pm(k)}(\rho, z_\pm)$ are

$$
\begin{cases}
H_{1n}^{\pm(k)}(z_\pm) = \frac{1}{\omega\mu\beta_n^\pm}\left[(\kappa_\pm^2 - \alpha_{2n}^2)E_{1n}^{\pm(k)}(z_\pm) + \alpha_{1n}\alpha_{2n}E_{2n}^{\pm(k)}(z_\pm)\right], \\
H_{2n}^{\pm(k)}(z_\pm) = \frac{1}{\omega\mu\beta_n^\pm}\left[(\kappa_\pm^2 - \alpha_{1n}^2)E_{2n}^{\pm(k)}(z_\pm) + \alpha_{1n}\alpha_{2n}E_{1n}^{\pm(k)}(z_\pm)\right].
\end{cases}
$$

Here $E_{1n}^{\pm(k)}(z_\pm)$ and $E_{2n}^{\pm(k)}(z_\pm)$ are the Fourier coefficients of $E_1^{\pm(k)}(\rho, z_\pm)$ and $E_1^{\pm(k)}(\rho, z_\pm)$, respectively.

Plugging (3.7) into the jump conditions (3.4) and (3.5) yields

$$\begin{cases} E_2^{+(k)} + \psi_y E_3^{+(k-1)} = E_2^{-(k)} + \psi_y E_3^{-(k-1)}, \\ E_1^{+(k)} + \psi_x E_3^{+(k-1)} = E_1^{-(k)} + \psi_x E_3^{-(k-1)}, \end{cases} \tag{3.11}$$

and

$$\begin{cases} \left(\partial_z E_1^{+(k)} + \psi_x \partial_z E_3^{+(k-1)} + \psi_y^2 \partial_z E_1^{+(k-2)} - \psi_x\psi_y \partial_z E_2^{+(k-2)}\right) \\ -z_-^{-1}\left(\partial_z E_1^{+(k-1)} + \psi_x \partial_z E_3^{+(k-2)} + \psi_y^2 \partial_z E_1^{+(k-3)} - \psi_x\psi_y \partial_z E_2^{+(k-3)}\right)\psi \\ -\left(\partial_x E_3^{+(k)} + \psi_y \partial_y E_1^{+(k-1)} - \psi_y \partial_x E_2^{+(k-1)}\right) \\ +\left(z_+^{-1} + z_-^{-1}\right)\left(\partial_x E_3^{+(k-1)} + \psi_y \partial_y E_1^{+(k-2)} - \psi_y \partial_x E_2^{+(k-2)}\right)\psi \\ -(z_+z_-)^{-1}\left(\partial_x E_3^{+(k-2)} + \psi_y \partial_y E_1^{+(k-3)} - \psi_y \partial_x E_2^{+(k-3)}\right)\psi^2 \\ = \left(\partial_z E_1^{-(k)} + \psi_x \partial_z E_3^{-(k-1)} + \psi_y^2 \partial_z E_1^{-(k-2)} - \psi_x\psi_y \partial_z E_2^{-(k-2)}\right) \\ -z_+^{-1}\left(\partial_z E_1^{-(k-1)} + \psi_x \partial_z E_3^{-(k-2)} + \psi_y^2 \partial_z E_1^{-(k-3)} - \psi_x\psi_y \partial_z E_2^{-(k-3)}\right)\psi \\ -\left(\partial_x E_3^{-(k)} + \psi_y \partial_y E_1^{-(k-1)} - \psi_y \partial_x E_2^{-(k-1)}\right) \\ +(z_+^{-1} + z_-^{-1})\left(\partial_x E_3^{-(k-1)} + \psi_y \partial_y E_1^{-(k-2)} - \psi_y \partial_x E_2^{-(k-2)}\right)\psi \\ -(z_+z_-)^{-1}\left(\partial_x E_3^{-(k-2)} + \psi_y \partial_y E_1^{-(k-3)} - \psi_y \partial_x E_2^{-(k-3)}\right)\psi^2 \\ \left(\partial_z E_2^{+(k)} + \psi_y \partial_z E_3^{+(k-1)} + \psi_x^2 \partial_z E_2^{+(k-2)} - \psi_x\psi_y \partial_z E_1^{+(k-2)}\right) \\ -z_-^{-1}\left(\partial_z E_2^{+(k-1)} + \psi_y \partial_z E_3^{+(k-2)} + \psi_x^2 \partial_z E_2^{+(k-3)} - \psi_x\psi_y \partial_z E_1^{+(k-3)}\right)\psi \\ -\left(\partial_y E_3^{+(k)} + \psi_x(\partial_x E_2^{+(k-1)} - \partial_y E_1^{+(k-1)})\right) \\ +(z_+^{-1} + z_-^{-1})\left(\partial_y E_3^{+(k-1)} + \psi_x \partial_x E_2^{+(k-2)} - \psi_x \partial_y E_1^{+(k-2)}\right)\psi \\ -(z_+z_-)^{-1}\left(\partial_y E_3^{+(k-2)} + \psi_x \partial_x E_2^{+(k-3)} - \psi_x \partial_y E_1^{+(k-3)}\right)\psi^2 \\ = \left(\partial_z E_2^{-(k)} + \psi_y \partial_z E_3^{-(k-1)} + \psi_x^2 \partial_z E_2^{-(k-2)} - \psi_x\psi_y \partial_z E_1^{-(k-2)}\right) \\ -z_+^{-1}\left(\partial_z E_2^{-(k-1)} + \psi_y \partial_z E_3^{-(k-2)} + \psi_x^2 \partial_z E_2^{-(k-3)} - \psi_x\psi_y \partial_z E_1^{-(k-3)}\right)\psi \\ -\left(\partial_y E_3^{-(k)} + \psi_x \partial_x E_2^{-(k-1)} - \psi_x \partial_y E_1^{-(k-1)}\right) \\ +(z_+^{-1} + z_-^{-1})\left(\partial_y E_3^{-(k-1)} + \psi_x \partial_x E_2^{-(k-2)} - \psi_x \partial_y E_1^{-(k-2)}\right)\psi \\ -(z_+z_-)^{-1}\left(\partial_y E_3^{-(k-2)} + \psi_x \partial_x E_2^{-(k-3)} - \psi_x \partial_y E_1^{-(k-3)}\right)\psi^2. \end{cases} \tag{3.12}$$

Substituting (3.7) into the divergence free condition (3.6) yields

$$\partial_x E_1^{\pm(k)} + \partial_y E_2^{\pm(k)} + \partial_z E_3^{\pm(k)} = g^{\pm(k)} \quad \text{in } D_\pm, \tag{3.13}$$

where

$$\begin{aligned} w^{\pm(k)} = {} & \frac{\psi}{z_\pm}\left(\partial_x E_1^{\pm(k-1)} + \partial_y E_2^{\pm(k-1)}\right) \\ & + \left(\frac{z_\pm - z}{z_\pm}\right)\left(\psi_x \partial_z E_1^{\pm(k-1)} + \psi_y \partial_z E_2^{\pm(k-1)}\right). \end{aligned}$$

3.3. Zeroth order

Recalling the recurrence relation (3.8) and letting $k = 0$, we have

$$\Delta E_j^{\pm(0)} + \kappa_\pm^2 E_j^{\pm(0)} = 0 \quad \text{in } D_\pm. \tag{3.14}$$

The transparent boundary conditions (3.9) and (3.10) becomes

$$\begin{cases} \partial_z E_1^{+(0)}(\rho, z_+) - \partial_x E_3^{+(0)}(\rho, z_+) = \mathrm{i}\omega\mu H_1^{+(0)}(\rho, z_+) + f_1(\rho), \\ \partial_z E_2^{+(0)}(\rho, z_+) - \partial_y E_3^{+(0)}(\rho, z_+) = \mathrm{i}\omega\mu H_2^{+(0)}(\rho, z_+) + f_2(\rho), \end{cases} \tag{3.15}$$

and

$$\begin{cases} \partial_z E_1^{-(0)}(\rho, z_-) - \partial_x E_3^{-(0)}(\rho, z_-) = -\mathrm{i}\omega\mu H_1^{-(0)}(\rho, z_-), \\ \partial_z E_2^{-(0)}(\rho, z_-) - \partial_y E_3^{-(0)}(\rho, z_-) = -\mathrm{i}\omega\mu H_2^{-(0)}(\rho, z_-). \end{cases} \tag{3.16}$$

The jump conditions (3.11) and (3.12) reduce to

$$E_2^{+(0)}(\rho, 0) = E_2^{-(0)}(\rho, 0), \quad E_1^{+(0)}(\rho, 0) = E_1^{-(0)}(\rho, 0), \tag{3.17}$$

and

$$\begin{cases} \partial_z E_1^{+(0)}(\rho, 0) - \partial_x E_3^{+(0)}(\rho, 0) = \partial_z E_1^{-(0)}(\rho, 0) - \partial_x E_3^{-(0)}(\rho, 0), \\ \partial_z E_2^{+(0)}(\rho, 0) - \partial_y E_3^{+(0)}(\rho, 0) = \partial_z E_2^{-(0)}(\rho, 0) - \partial_y E_3^{-(0)}(\rho, 0). \end{cases} \tag{3.18}$$

The divergence free condition (3.13) reduces to

$$\partial_x E_1^{\pm(0)} + \partial_y E_2^{\pm(0)} + \partial_z E_3^{\pm(0)} = 0 \quad \text{in } D_\pm. \tag{3.19}$$

Since $E_j^{\pm(0)}(\rho, z)$ and f_j are periodic functions of ρ with period Λ, they have the following Fourier expansion

$$E_j^{\pm(0)}(\rho, z) = \sum_{n\in\mathbb{Z}^2} E_{jn}^{\pm(0)}(z)\mathrm{e}^{\mathrm{i}\alpha_n\cdot\rho}, \quad f_j(\rho) = \sum_{n\in\mathbb{Z}^2} f_{jn}\mathrm{e}^{\mathrm{i}\alpha_n\cdot\rho}, \tag{3.20}$$

where

$$f_{jn} = \begin{cases} -2\mathrm{i}\kappa_+ p_j \mathrm{e}^{-\mathrm{i}\kappa_+ z_+} & \text{for} \quad n = 0, \\ 0 & \text{for} \quad n \neq 0. \end{cases}$$

Plugging (3.20) into (3.14)–(3.19), we obtain an ordinary differential equation

$$\frac{\mathrm{d}^2 E_{jn}^{\pm(0)}(z)}{\mathrm{d}z^2} + (\beta_n^\pm)^2 E_{jn}^{\pm(0)}(z) = 0, \tag{3.21}$$

together with the boundary conditions at $z = z_+$:

$$\begin{cases} E_{1n}^{+(0)\prime} - \mathrm{i}\alpha_{1n} E_{3n}^{+(0)} = \frac{\mathrm{i}}{\beta_n^+}\left[(\kappa_+^2 - \alpha_{2n}^2)E_{1n}^{+(0)} + \alpha_{1n}\alpha_{2n}E_{2n}^{+(0)}\right] + f_{1n}, \\ E_{2n}^{+(0)\prime} - \mathrm{i}\alpha_{2n} E_{3n}^{+(0)} = \frac{\mathrm{i}}{\beta_n^+}\left[(\kappa_+^2 - \alpha_{1n}^2)E_{2n}^{+(0)} + \alpha_{1n}\alpha_{2n}E_{1n}^{+(0)}\right] + f_{2n}, \\ E_{3n}^{+(0)\prime} + \mathrm{i}\alpha_{1n} E_{1n}^{+(0)} + \mathrm{i}\alpha_{2n} E_{2n}^{+(0)} = 0. \end{cases} \tag{3.22}$$

and the boundary conditions at $z = z_-$:

$$\begin{cases} E_{1n}^{-(0)\prime} - \mathrm{i}\alpha_{1n}E_{3n}^{-(0)} = -\frac{\mathrm{i}}{\beta_n^-}\left[(\kappa_-^2 - \alpha_{2n}^2)E_{1n}^{-(0)} + \alpha_{1n}\alpha_{2n}E_{2n}^{-(0)}\right], \\ E_{2n}^{-(0)\prime} - \mathrm{i}\alpha_{2n}E_{3n}^{-(0)} = -\frac{\mathrm{i}}{\beta_n^-}\left[(\kappa_-^2 - \alpha_{1n}^2)E_{2n}^{-(0)} + \alpha_{1n}\alpha_{2n}E_{1n}^{-(0)}\right], \\ E_{3n}^{-(0)\prime} + \mathrm{i}\alpha_{1n}E_{1n}^{-(0)} + \mathrm{i}\alpha_{2n}E_{2n}^{-(0)} = 0, \end{cases} \tag{3.23}$$

and the jump conditions at $z = 0$:

$$E_{2n}^{+(0)} = E_{2n}^{-(0)}, \quad E_{1n}^{+(0)} = E_{1n}^{-(0)}, \tag{3.24}$$

and

$$\begin{cases} E_{1n}^{+(0)\prime} - \mathrm{i}\alpha_{1n}E_{3n}^{+(0)} = E_{1n}^{-(0)\prime} - \mathrm{i}\alpha_{1n}E_{3n}^{-(0)}, \\ E_{2n}^{+(0)\prime} - \mathrm{i}\alpha_{2n}E_{3n}^{+(0)} = E_{2n}^{-(0)\prime} - \mathrm{i}\alpha_{2n}E_{3n}^{-(0)}. \end{cases} \tag{3.25}$$

It can be verified that the general solutions of the homogeneous second order equations (3.21) are

$$E_{jn}^{\pm(0)}(z) = A_{jn}^{\pm}\mathrm{e}^{\mathrm{i}\beta_n^{\pm}z} + B_{jn}^{\pm}\mathrm{e}^{-\mathrm{i}\beta_n^{\pm}z}, \tag{3.26}$$

where $A_{jn}^{\pm}, B_{jn}^{\pm} \in \mathbb{C}$ are to be determined. Substituting (3.26) into the boundary conditions (3.22) and (3.23), and the jump conditions (3.24) and (3.25), we may deduce that

$$A_{j0}^{+(0)} = rp_j, \quad B_{j0}^{+(0)} = p_j, \quad A_{j0}^{-(0)} = 0, \quad B_{j0}^{-(0)} = tp_j,$$

and $A_{jn}^{\pm} = B_{jn}^{\pm} = A_{jn}^{\pm} = B_{jn}^{\pm} = 0$ for $n \neq 0$, where

$$r = \frac{\kappa_+ - \kappa_-}{\kappa_+ + \kappa_-} \quad \text{and} \quad t = \frac{2\kappa_+}{\kappa_+ + \kappa_-}$$

are known as the reflection coefficient and the transmission coefficient, respectively. Hence we find the analytic expressions for the zeroth order terms:

$$\begin{cases} E_j^{+(0)}(\rho, z) = p_j(\mathrm{e}^{-\mathrm{i}\kappa_+ z} + r\mathrm{e}^{\mathrm{i}\kappa_+ z}), \\ E_j^{-(0)}(\rho, z) = p_j t\mathrm{e}^{-\mathrm{i}\kappa_- z}. \end{cases} \tag{3.27}$$

Clearly, the zeroth order terms consist of the incident wave, the reflected wave, and the transmitted wave, which come from the diffraction of an electromagnetic plane wave by a planar surface.

3.4. First order

In this section, we derive analytic expressions of the first order terms, and particularly a connection between their Fourier coefficients and the Fourier coefficient of the grating profile.

Taking $k = 1$ in (3.8) yields

$$\Delta E_j^{\pm(1)} + \kappa^2 E_j^{\pm(1)} = F_j^{\pm(1)} \quad \text{in } D_{\pm}, \tag{3.28}$$

where

$$F_j^{\pm(1)} = \frac{2\psi}{z_\pm}\frac{\partial^2 E_j^{\pm(0)}}{\partial x^2} + \frac{2\psi}{z_\pm}\frac{\partial^2 E_j^{\pm(0)}}{\partial y^2} + \frac{2(z_\pm - z)\psi_x}{z_\pm}\frac{\partial^2 E_j^{\pm(0)}}{\partial x \partial z} + \frac{2(z_\pm - z)\psi_y}{z_\pm}\frac{\partial^2 E_j^{\pm(0)}}{\partial y \partial z} + \frac{(z_\pm - z)(\psi_{xx} + \psi_{yy})}{z_\pm}\frac{\partial E_j^{\pm(0)}}{\partial z} + \frac{2\kappa_\pm^2 \psi}{z_\pm} E_j^{\pm(0)}.$$

It follows from the explicit expression of the zeroth order term (3.27) that we have

$$F_j^{+(1)}(\rho, z) = \frac{2\kappa_+^2 p_j}{z_+}\left(\mathrm{e}^{-\mathrm{i}\kappa_+ z} + r e^{\mathrm{i}\kappa_+ z}\right)\psi - \frac{\mathrm{i}\kappa_+ p_j (z_+ - z)}{z_+}\left(\mathrm{e}^{-\mathrm{i}\kappa_+ z} - r e^{\mathrm{i}\kappa_+ z}\right)(\psi_{xx} + \psi_{yy})$$

and

$$F_j^{-(1)}(\rho, z) = \frac{2\kappa_-^2 p_j}{z_-} t\mathrm{e}^{-\mathrm{i}\kappa_- z}\psi - \frac{\mathrm{i}\kappa_- p_j (z_- - z)}{z_-} t\mathrm{e}^{-\mathrm{i}\kappa_- z}(\psi_{xx} + \psi_{yy}).$$

The transparent boundary conditions (3.9) and (3.10) become

$$\begin{cases} \partial_z E_1^{+(1)}(\rho, z_+) - \partial_x E_3^{+(1)}(\rho, z_+) = \mathrm{i}\omega\mu H_1^{+(1)}(\rho, z_+) - f_1^{+(1)}(\rho), \\ \partial_z E_2^{+(1)}(\rho, z_+) - \partial_y E_3^{+(1)}(\rho, z_+) = \mathrm{i}\omega\mu H_2^{+(1)}(\rho, z_+) - f_2^{+(1)}(\rho), \end{cases} \tag{3.29}$$

and

$$\begin{cases} \partial_z E_1^{-(1)}(\rho, z_-) - \partial_x E_3^{-(1)}(\rho, z_-) = -\mathrm{i}\omega\mu H_1^{-(1)}(\rho, z_-) - f_1^{-(1)}(\rho), \\ \partial_z E_2^{-(1)}(\rho, z_-) - \partial_y E_3^{-(1)}(\rho, z_-) = -\mathrm{i}\omega\mu H_2^{-(1)}(\rho, z_-) - f_2^{-(1)}(\rho), \end{cases} \tag{3.30}$$

where we have from (3.27) that

$$f_j^{+(1)}(\rho) = \frac{\psi}{z_+}\partial_z E_j^{+(0)}(\rho, z_+) = -\frac{\mathrm{i}\kappa_+ p_j}{z_+}\left(\mathrm{e}^{-\mathrm{i}\kappa_+ z_+} - r e^{\mathrm{i}\kappa_+ z_+}\right)\psi,$$
$$f_j^{-(1)}(\rho) = \frac{\psi}{z_-}\partial_z E_j^{-(0)}(\rho, z_-) = -\frac{\mathrm{i}\kappa_- p_j}{z_-} t\mathrm{e}^{-\mathrm{i}\kappa_- z_-}\psi.$$

The jump conditions (3.11) and (3.12) reduce to

$$\begin{cases} E_2^{+(1)} + \psi_y E_3^{+(0)} = E_2^{-(1)} + \psi_y E_3^{-(0)}, \\ E_1^{+(1)} + \psi_x E_3^{+(0)} = E_1^{-(1)} + \psi_x E_3^{-(0)}, \end{cases}$$

and

$$\begin{cases} \partial_z E_1^{+(1)} - \frac{\psi}{z_-}\partial_z E_1^{+(0)} - \partial_x E_3^{+(1)} = \partial_z E_1^{-(1)} - \frac{\psi}{z_+}\partial_z E_1^{-(0)} - \partial_x E_3^{-(1)}, \\ \partial_z E_2^{+(1)} - \frac{\psi}{z_-}\partial_z E_2^{+(0)} - \partial_y E_3^{+(1)} = \partial_z E_2^{-(1)} - \frac{\psi}{z_+}\partial_z E_2^{-(0)} - \partial_y E_3^{-(1)}, \end{cases}$$

which gives after substitution of (3.27) that

$$E_2^{+(1)} = E_2^{-(1)}, \quad E_1^{+(1)} = E_1^{-(1)}, \tag{3.31}$$

and

$$\begin{cases} \partial_z E_1^{+(1)} - \partial_x E_3^{+(1)} + \frac{\mathrm{i}\kappa_+ p_1}{z_-}(1-r)\psi = \partial_z E_1^{-(1)} - \partial_x E_3^{-(1)} + \frac{\mathrm{i}\kappa_- p_1}{z_+} t\psi, \\ \partial_z E_2^{+(1)} - \partial_y E_3^{+(1)} + \frac{\mathrm{i}\kappa_+ p_2}{z_-}(1-r)\psi = \partial_z E_2^{-(1)} - \partial_y E_3^{-(1)} + \frac{\mathrm{i}\kappa_- p_2}{z_+} t\psi. \end{cases} \tag{3.32}$$

The divergence free condition (3.13) reduces to

$$\partial_x E_1^{\pm(1)} + \partial_y E_2^{\pm(1)} + \partial_z E_3^{\pm(1)} = g^{\pm(1)} \quad \text{in } D_\pm, \tag{3.33}$$

where

$$g^{\pm(1)}(\rho, z) = \frac{\psi}{z_\pm}\left(\partial_x E_1^{\pm(0)} + \partial_y E_2^{\pm(0)}\right) + \left(\frac{z_\pm - z}{z_\pm}\right)\left(\psi_x \partial_z E_1^{\pm(0)} + \psi_y \partial_z E_2^{\pm(0)}\right).$$

Using (3.27), we get

$$g^{+(1)}(\rho, z) = -\frac{\mathrm{i}\kappa_+(z_+ - z)}{z_+}\left(\mathrm{e}^{-\mathrm{i}\kappa_+ z} - r e^{\mathrm{i}\kappa_+ z}\right)(p_1\psi_x + p_2\psi_y)$$

and

$$g^{-(1)}(\rho, z) = -\frac{\mathrm{i}\kappa_-(z_- - z)}{z_-} t\mathrm{e}^{-\mathrm{i}\kappa_- z}(p_1\psi_x + p_2\psi_y).$$

Since $\psi(\rho)$, $E_j^{\pm(1)}(\rho, z)$, and $F_j^{\pm(1)}(\rho, z)$ are periodic functions of ρ with period Λ, they have the following Fourier expansions

$$\begin{aligned} \psi(\rho) &= \sum_{n\in\mathbb{Z}^2} \psi_n \mathrm{e}^{\mathrm{i}\alpha_n\cdot\rho}, \\ E_j^{\pm(1)}(\rho, z) &= \sum_{n\in\mathbb{Z}^2} E_{jn}^{\pm(1)}(z)\mathrm{e}^{\mathrm{i}\alpha_n\cdot\rho}, \\ F_j^{\pm(1)}(\rho, z) &= \sum_{n\in\mathbb{Z}^2} F_{jn}^{\pm(1)}(z)\mathrm{e}^{\mathrm{i}\alpha_n\cdot\rho} \end{aligned}$$

where

$$\begin{aligned} F_{jn}^{+(1)}(z) = \Big[&\frac{2\kappa_+^2 p_j}{z_+}\left(\mathrm{e}^{-\mathrm{i}\kappa_+ z} + r e^{\mathrm{i}\kappa_+ z}\right) \\ &+ \frac{\mathrm{i}\kappa_+ p_j(z_+ - z)}{z_+}(\alpha_{1n}^2 + \alpha_{2n}^2)\left(\mathrm{e}^{-\mathrm{i}\kappa_+ z} - r\mathrm{e}^{\mathrm{i}\kappa_+ z}\right)\Big]\psi_n \end{aligned}$$

and

$$F_{jn}^{-(1)}(z) = \left[\frac{2\kappa_-^2 p_j}{z_-} t\mathrm{e}^{-\mathrm{i}\kappa_- z} + \frac{\mathrm{i}\kappa_- p_j(z_- - z)}{z_-}(\alpha_{1n}^2 + \alpha_{2n}^2) t\mathrm{e}^{-\mathrm{i}\kappa_- z}\right]\psi_n.$$

Plugging the above Fourier expansions into (3.28) and using (3.29)–(3.33), we derive an ordinary differential equation

$$\frac{\mathrm{d}^2 E_{jn}^{\pm(1)}(z)}{\mathrm{d}z^2} + (\beta_n^\pm)^2 E_{jn}^{\pm(1)}(z) = F_{jn}^{\pm(1)}(z), \tag{3.34}$$

together with the boundary conditions at $z = z_+$:

$$\begin{cases} E_{1n}^{+(1)\prime} - \mathrm{i}\alpha_{1n}E_{3n}^{+(1)} = \frac{\mathrm{i}}{\beta_n^+}\left[(\kappa_+^2 - \alpha_{2n}^2)E_{1n}^{+(1)} + \alpha_{1n}\alpha_{2n}E_{2n}^{+(1)}\right] - f_{1n}^{+(1)}, \\ E_{2n}^{+(1)\prime} - \mathrm{i}\alpha_{2n}E_{3n}^{+(1)} = \frac{\mathrm{i}}{\beta_n^+}\left[(\kappa_+^2 - \alpha_{1n}^2)E_{2n}^{+(1)} + \alpha_{1n}\alpha_{2n}E_{1n}^{+(1)}\right] - f_{2n}^{+(1)} \\ E_{3n}^{+(1)\prime} + \mathrm{i}\alpha_{1n}E_{1n}^{+(1)} + \mathrm{i}\alpha_{2n}E_{2n}^{+(1)} = 0, \end{cases} \tag{3.35}$$

and the boundary conditions at $z = z_-$:

$$\begin{cases} E_{1n}^{-(1)\prime} - \mathrm{i}\alpha_{1n}E_{3n}^{-(1)} = -\frac{\mathrm{i}}{\beta_n^-}\left[(\kappa_-^2 - \alpha_{2n}^2)E_{1n}^{-(1)} + \alpha_{1n}\alpha_{2n}E_{2n}^{-(1)}\right] - f_{1n}^{-(1)}, \\ E_{2n}^{-(1)\prime} - \mathrm{i}\alpha_{2n}E_{3n}^{-(1)} = -\frac{\mathrm{i}}{\beta_n^-}\left[(\kappa_-^2 - \alpha_{1n}^2)E_{2n}^{-(1)} + \alpha_{1n}\alpha_{2n}E_{1n}^{-(1)}\right] - f_{2n}^{-(1)} \\ E_{3n}^{-(1)\prime} + \mathrm{i}\alpha_{1n}E_{1n}^{-(1)} + \mathrm{i}\alpha_{2n}E_{2n}^{-(1)} = 0, \end{cases} \tag{3.36}$$

where $f_{jn}^{\pm(1)}$ are the Fourier coefficients of $f_j^{\pm(1)}(\rho)$. Explicitly, we have

$$\begin{aligned} f_{jn}^{+(1)} &= -\frac{\mathrm{i}\kappa_+ p_j}{z_+}\left(\mathrm{e}^{-\mathrm{i}\kappa_+ z_+} - r\mathrm{e}^{\mathrm{i}\kappa_+ z_+}\right)\psi_n, \\ f_{jn}^{-(1)} &= -\frac{\mathrm{i}\kappa_- p_j}{z_-} t\mathrm{e}^{-\mathrm{i}\kappa_- z_-}\psi_n. \end{aligned}$$

Using the identity $\kappa_+(1-r) = \kappa_- t$, we may reduce the jump conditions (3.31) and (3.32) to

$$E_{2n}^{+(1)} = E_{2n}^{-(1)}, \quad E_{1n}^{+(1)} = E_{1n}^{-(1)}, \tag{3.37}$$

and

$$\begin{cases} E_{1n}^{+(1)\prime} - \mathrm{i}\alpha_{1n}E_{3n}^{+(1)} = E_{1n}^{-(1)\prime} - \mathrm{i}\alpha_{1n}E_{3n}^{-(1)} + \mathrm{i}\kappa_- t p_1\left(z_+^{-1} - z_-^{-1}\right)\psi_n, \\ E_{2n}^{+(1)\prime} - \mathrm{i}\alpha_{2n}E_{3n}^{+(1)} = E_{2n}^{-(1)\prime} - \mathrm{i}\alpha_{2n}E_{3n}^{-(1)} + \mathrm{i}\kappa_- t p_2\left(z_+^{-1} - z_-^{-1}\right)\psi_n. \end{cases} \tag{3.38}$$

Based on the same identity $\kappa_+(1-r) = \kappa_- t$, we may obtain two more conditions at $z = 0$ from (3.33):

$$\begin{cases} E_{3n}^{+(1)\prime} + \mathrm{i}\alpha_{1n}E_{1n}^{+(1)} + \mathrm{i}\alpha_{2n}E_{2n}^{+(1)} = \kappa_- t(\alpha_{1n}p_1 + \alpha_{2n}p_2)\psi_n, \\ E_{3n}^{-(1)\prime} + \mathrm{i}\alpha_{1n}E_{1n}^{-(1)} + \mathrm{i}\alpha_{2n}E_{2n}^{-(1)} = \kappa_- t(\alpha_{1n}p_1 + \alpha_{2n}p_2)\psi_n. \end{cases} \tag{3.39}$$

It follows from (3.34) that the general solutions of $E_{jn}^{\pm(1)}$ consist of the general solution for the corresponding homogeneous equation and a particular solution for the non-homogeneous equation:

$$E_{jn}^{+(1)}(z) = A_{jn}^+\mathrm{e}^{\mathrm{i}\beta_n^+ z} + B_{jn}^+\mathrm{e}^{-\mathrm{i}\beta_n^+ z} - \frac{\mathrm{i}\kappa_+ p_j}{z_+}(z_+ - z)\left(\mathrm{e}^{-\mathrm{i}\kappa_+ z} - r\mathrm{e}^{\mathrm{i}\kappa_+ z}\right)\psi_n \tag{3.40}$$

and

$$E_{jn}^{-(1)}(z) = A_{jn}^-\mathrm{e}^{\mathrm{i}\beta_n^- z} + B_{jn}^-\mathrm{e}^{-\mathrm{i}\beta_n^- z} - \frac{\mathrm{i}\kappa_- p_j}{z_-}(z_- - z)t\mathrm{e}^{-\mathrm{i}\kappa_- z}\psi_n. \tag{3.41}$$

Plugging (3.40) and (3.41) into (3.35) and (3.36), and using the identity $\kappa_\pm^2 = (\beta_n^\pm)^2 + \alpha_{1n}^2 + \alpha_{2n}^2$, we obtain

$$\begin{cases} \alpha_{1n}^2 A_{1n}^+ + [2(\beta_n^+)^2 + \alpha_{1n}^2]\mathrm{e}^{-2\mathrm{i}\beta_n^+ z_+} B_{1n}^+ + \alpha_{1n}\alpha_{2n} A_{2n}^+ \\ \qquad +\alpha_{1n}\alpha_{2n}\mathrm{e}^{-2\mathrm{i}\beta_n^+ z_+} B_{2n}^+ = -\alpha_{1n}\beta_n^+ A_{3n}^+ - \alpha_{1n}\beta_n^+ \mathrm{e}^{-2\mathrm{i}\beta_n^+ z_+} B_{3n}^+, \\ \alpha_{2n}^2 A_{2n}^+ + [2(\beta_n^+)^2 + \alpha_{2n}^2]\mathrm{e}^{-2\mathrm{i}\beta_n^+ z_+} B_{2n}^+ + \alpha_{1n}\alpha_{2n} A_{1n}^+ \\ \qquad +\alpha_{1n}\alpha_{2n}\mathrm{e}^{-2\mathrm{i}\beta_n^+ z_+} B_{1n}^+ = -\alpha_{2n}\beta_n A_{3n}^+ - \alpha_{2n}\beta_n^+ \mathrm{e}^{-2\mathrm{i}\beta_n^+ z_+} B_{3n}^+, \\ \alpha_{1n} A_{1n}^+ + \alpha_{1n}\mathrm{e}^{-2\mathrm{i}\beta_n^+ z_+} B_{1n}^+ + \alpha_{2n} A_{2n}^+ + \alpha_{2n}\mathrm{e}^{-2\mathrm{i}\beta_n^+ z_+} B_{2n}^+ \\ \qquad = -\beta_n^+ A_{3n}^+ + \beta_n^+ \mathrm{e}^{-2\mathrm{i}\beta_n^+ z_+} B_{3n}^+ \end{cases} \tag{3.42}$$

and

$$\begin{cases} [2(\beta_n^-)^2 + \alpha_{1n}^2] A_{1n}^- + \alpha_{1n}^2 \mathrm{e}^{-2\mathrm{i}\beta_n^- z_-} B_{1n}^- + \alpha_{1n}\alpha_{2n} A_{2n}^- \\ \qquad +\alpha_{1n}\alpha_{2n}\mathrm{e}^{-2\mathrm{i}\beta_n^- z_-} B_{2n}^- = \alpha_{1n}\beta_n^- A_{3n}^- + \alpha_{1n}\beta_n^- \mathrm{e}^{-2\mathrm{i}\beta_n^- z_-} B_{3n}^-, \\ [2(\beta_n^-)^2 + \alpha_{2n}^2] A_{2n}^- + \alpha_{2n}^2 \mathrm{e}^{-2\mathrm{i}\beta_n^- z_-} B_{2n}^- + \alpha_{1n}\alpha_{2n} A_{1n}^- \\ \qquad +\alpha_{1n}\alpha_{2n}\mathrm{e}^{-2\mathrm{i}\beta_n^- z_-} B_{1n}^- = \alpha_{2n}\beta_n^- A_{3n}^- + \alpha_{2n}\beta_n^- \mathrm{e}^{-2\mathrm{i}\beta_n^- z_-} B_{3n}^-, \\ \alpha_{1n} A_{1n}^- + \alpha_{1n}\mathrm{e}^{-2\mathrm{i}\beta_n^- z_-} B_{1n}^- + \alpha_{2n} A_{2n}^- + \alpha_{2n}\mathrm{e}^{-2\mathrm{i}\beta_n^- z_-} B_{2n}^- \\ \qquad = -\beta_n^- A_{3n}^- + \beta_n^- \mathrm{e}^{-2\mathrm{i}\beta_n^- z_-} B_{3n}^-. \end{cases} \tag{3.43}$$

Multiplying individually α_{1n} and α_{2n} on both sides of the third equation in (3.42) and (3.43), and subtracting them from the first and second equation, respectively, we get

$$B_{1n}^+ = -\frac{\alpha_{1n}}{\beta_n^+} B_{3n}^+, \quad B_{2n}^+ = -\frac{\alpha_{2n}}{\beta_n^+} B_{3n}^+, \quad A_{1n}^- = \frac{\alpha_{1n}}{\beta_n^-} A_{3n}^-, \quad A_{2n}^- = \frac{\alpha_{2n}}{\beta_n^-} A_{3n}^-. \tag{3.44}$$

Substituting (3.44) into the third equations in (3.42) and (3.43) yields

$$\begin{cases} \alpha_{1n} A_{1n}^+ + \alpha_{2n} A_{2n}^+ = \frac{\kappa_+^2}{\beta_n^+}\mathrm{e}^{-2\mathrm{i}\beta_n^+ z_+} B_{3n}^+ - \beta_n^+ A_{3n}^+, \\ \alpha_{1n} B_{1n}^- + \alpha_{2n} B_{2n}^- = \beta_n^- B_{3n}^- - \frac{\kappa_-^2}{\beta_n^-}\mathrm{e}^{2\mathrm{i}\beta_n^- z_-} A_{3n}^-. \end{cases} \tag{3.45}$$

Substituting (3.44), (3.40), and (3.41) into (3.39), we get

$$\begin{cases} \alpha_{1n} A_{1n}^+ + \alpha_{2n} A_{2n}^+ = \frac{\kappa_+^2}{\beta_n^+} B_{3n}^+ - \beta_n^+ A_{3n}^+, \\ \alpha_{1n} B_{1n}^- + \alpha_{2n} B_{2n}^- = \beta_n^- B_{3n}^- - \frac{\kappa_-^2}{\beta_n^-} A_{3n}^-. \end{cases} \tag{3.46}$$

Combining (3.44)–(3.46) gives

$$B_{1n}^+ = B_{2n}^+ = B_{3n}^+ = 0 \quad \text{and} \quad A_{1n}^- = A_{2n}^- = A_{3n}^- = 0. \tag{3.47}$$

Plugging (3.47), (3.40), and (3.41) into (3.37) and (3.38), we obtain

$$\begin{cases} A_{1n}^+ - B_{1n}^- = 0, \\ \beta_n^+ A_{1n}^+ + \beta_n^- B_{1n}^- = \alpha_{1n}(A_{3n}^+ - B_{3n}^-) - 2\mathrm{i}\kappa_+(\kappa_+ - \kappa_-)\, p_1 \psi_n, \end{cases} \tag{3.48}$$

and

$$\begin{cases} A_{2n}^{+} - B_{2n}^{-} = 0, \\ \beta_n^{+} A_{2n}^{+} + \beta_n^{-} B_{2n}^{-} = \alpha_{2n}(A_{3n}^{+} - B_{3n}^{-}) - 2\mathrm{i}\kappa_{+}(\kappa_{+} - \kappa_{-})\, p_2 \psi_n. \end{cases} \tag{3.49}$$

Upon solving (3.48) and (3.49), we have

$$\begin{cases} A_{1n}^{+} = B_{1n}^{-} = (\beta_n^{+} + \beta_n^{-})^{-1} \left[\alpha_{1n}(A_{3n}^{+} - B_{3n}^{-}) - 2\mathrm{i}\kappa_{+}(\kappa_{+} - \kappa_{-})\, p_1 \psi_n\right], \\ A_{2n}^{+} = B_{2n}^{-} = (\beta_n^{+} + \beta_n^{-})^{-1} \left[\alpha_{2n}(A_{3n}^{+} - B_{3n}^{-}) - 2\mathrm{i}\kappa_{+}(\kappa_{+} - \kappa_{-})\, p_2 \psi_n\right]. \end{cases} \tag{3.50}$$

Substituting (3.50) into (3.46) and noting (3.47), we may derive after tedious calculations that

$$\begin{cases} A_{3n}^{+} = \frac{2\mathrm{i}\beta_n^{-}\kappa_{+}(\kappa_{+}-\kappa_{-})(p_1\alpha_{1n}+p_2\alpha_{2n})}{(\beta_n^{+}+\beta_n^{-})(\alpha_{1n}^2+\alpha_{2n}^2+\beta_n^{+}\beta_n^{-})}\psi_n, \\ B_{3n}^{-} = -\frac{2\mathrm{i}\beta_n^{+}\kappa_{+}(\kappa_{+}-\kappa_{-})(p_1\alpha_{1n}+p_2\alpha_{2n})}{(\beta_n^{+}+\beta_n^{-})(\alpha_{1n}^2+\alpha_{2n}^2+\beta_n^{+}\beta_n^{-})}\psi_n. \end{cases} \tag{3.51}$$

Plugging (3.51) into (3.50) yields

$$A_{1n}^{+} = B_{1n}^{-} = C_{1n}\psi_n, \quad A_{2n}^{+} = B_{2n}^{-} = C_{2n}\psi_n, \tag{3.52}$$

where

$$\begin{cases} C_{1n} = \frac{2\mathrm{i}\kappa_{+}(\kappa_{+}-\kappa_{-})}{(\beta_n^{+}+\beta_n^{-})}\left[\frac{\alpha_{1n}(p_1\alpha_{1n}+p_2\alpha_{2n})}{(\alpha_{1n}^2+\alpha_{2n}^2+\beta_n^{+}\beta_n^{-})} - p_1\right], \\ C_{2n} = \frac{2\mathrm{i}\kappa_{+}(\kappa_{+}-\kappa_{-})}{(\beta_n^{+}+\beta_n^{-})}\left[\frac{\alpha_{2n}(p_1\alpha_{1n}+p_2\alpha_{2n})}{(\alpha_{1n}^2+\alpha_{2n}^2+\beta_n^{+}\beta_n^{-})} - p_2\right]. \end{cases}$$

Substituting (3.47) and (3.52) into (3.40) and (3.41), and evaluating at z_+ and z_-, respectively, we obtain

$$E_{jn}^{+(1)}(z_+) = C_{jn}\mathrm{e}^{\mathrm{i}\beta_n^{+}z_+}\psi_n, \quad E_{jn}^{-(1)}(z_-) = C_{jn}\mathrm{e}^{-\mathrm{i}\beta_n^{-}z_-}\psi_n. \tag{3.53}$$

4. Reconstruction formula

In this section, we present an explicit reconstruction formula for the inverse grating surface problem by using the scattering data.

Assume that the noisy data takes the form

$$E_j^{\pm\gamma}(\rho, z_\pm) = E_j^{\pm}(\rho, z_\pm) + \mathcal{O}(\gamma),$$

where $E_j^{\pm}(\rho, z_\pm)$, $j = 1, 2$ are the exact data and γ is the noise level.

Evaluating the power series (3.7) at $z = z_\pm$ and replacing $E_j^{\pm}(\rho, z_\pm)$ with the noisy data $E_j^{\pm\gamma}(\rho, z_\pm)$, we have

$$E_j^{\pm\gamma}(\rho, z_\pm) = E_j^{\pm(0)}(\rho, z_\pm) + \delta E_j^{\pm(1)}(\rho, z_\pm) + \mathcal{O}(\delta^2) + \mathcal{O}(\gamma). \tag{4.1}$$

Rearranging (4.1), and dropping $\mathcal{O}(\delta^2)$ and $\mathcal{O}(\gamma)$ yield

$$\delta E_j^{\pm(1)}(\rho, z_\pm) = E_j^{\pm\gamma}(\rho, z_\pm) - E_j^{\pm(0)}(\rho, z_\pm) \tag{4.2}$$

which is the linearization of the nonlinear inverse problem and enables us to find an explicit reconstruction formula for the linearized inverse problem.

Noting $\phi = \delta\psi$ and thus $\phi_n = \delta\psi_n$, where ϕ_n is the Fourier coefficient of ϕ. Plugging (3.53) into (4.2), we may deduce that

$$\phi_n = C_{jn}^{-1}\left[E_{jn}^{\pm\gamma}(z_\pm) - E_{jn}^{\pm(0)}(z_\pm)\right] \mathrm{e}^{\mp \mathrm{i}\beta_n^\pm z_\pm}, \tag{4.3}$$

where $E_{jn}^{\pm\gamma}(z_\pm)$ is the Fourier coefficient of the noisy data $E_j^{\pm\gamma}(\rho, z_\pm)$ and $E_{jn}^{\pm(0)}(z_\pm)$ is the Fourier coefficient of $E_j^{\pm(0)}(\rho, z_\pm)$ given as

$$E_{jn}^{+(0)}(z_+) = p_j(\mathrm{e}^{-\mathrm{i}\kappa_+ z_+} + r\mathrm{e}^{\mathrm{i}\kappa_+ z_+})\delta_{0n} \quad \text{and} \quad E_{jn}^{-(0)}(z_-) = p_j t\mathrm{e}^{-\mathrm{i}\kappa_- z_-}\delta_{0n}. \tag{4.4}$$

Here δ_{0n} the Kronecker's delta function.

It follows from (4.3) and the definitions of $\beta_n^\pm$ in (2.6) and (2.9) that it is well-posed to reconstruct those Fourier coefficients ϕ_n with $|\alpha_n| < \kappa_\pm$, since the small variations of the measured data will not be amplified and lead to large errors in the reconstruction, but the resolution of the reconstructed function f is restricted by the given wavenumber $\kappa_\pm$. In contrast, it is severely ill-posed to reconstruct those Fourier coefficients ϕ_n with $|\alpha_n| > \kappa_\pm$, since the small variations in the data will be exponentially enlarged and lead to huge errors in the reconstruction, but they contribute to the super resolution of the reconstructed function ϕ.

To obtain a stable and super-resolved reconstruction, we adopt a regularization to suppress the exponential growth of the reconstruction errors. Besides, we may use as small $|z_\pm|$ as possible, i.e. measure the data at the distance which is as close as possible to the grating surface which is exactly the idea of near-field optics.

We consider the spectral cut-off regularization. Define the signal-to-noise ratio (SNR) by

$$\mathrm{SNR} = \min\{\delta^{-2},\ \gamma^{-1}\}.$$

For fixed $z_\pm$, the cut-off frequency $\omega_\pm$ is chosen in such a way that

$$\mathrm{e}^{|z_\pm|(\omega_\pm^2 - \kappa_\pm^2)^{1/2}} = \mathrm{SNR},$$

which implies that the spatial frequency will be cut-off for those below the noise level. More explicitly, we have

$$\frac{\omega_\pm}{\kappa_\pm} = \left[1 + \left(\frac{\log \mathrm{SNR}}{\kappa_\pm |z_\pm|}\right)^2\right]^{1/2}, \tag{4.5}$$

which indicates $\omega_\pm > \kappa_\pm$ as long as $\mathrm{SNR} > 0$. The cut-off frequency $\omega_\pm$ determines the highest Fourier mode which can be recovered from the reconstruction. As is shown in (4.5), the cut-off frequency $\omega_\pm$ is an increasing function of SNR and a decreasing function of the measurement distance $|z_\pm|$; larger SNR or smaller $|z_\pm|$ may help to achieve better resolution of the reconstruction.

Taking into account the frequency cut-off, we may have a regularized reconstruction formulation for (4.3):

$$\phi_n = C_{jn}^{-1}\left[E_{jn}^{\pm\gamma}(z_\pm) - E_{jn}^{\pm(0)}(z_\pm)\right] \mathrm{e}^{\mp \mathrm{i}\beta_n^\pm z_\pm}\, \chi_n^\pm,$$

where the characteristic function

$$\chi_n^\pm = \begin{cases} 1 & \text{for} \quad |\alpha_n| \leqslant \omega_\pm, \\ 0 & \text{for} \quad |\alpha_n| > \omega_\pm. \end{cases}$$

Once ϕ_n are computed, the grating surface function can be approximated by

$$\phi(\rho) \approx \sum_{n\in\mathbb{Z}} \phi_n \mathrm{e}^{\mathrm{i}\alpha_n\cdot\rho} = \sum_{|\alpha_n|\leqslant\omega_\pm} C_{jn}^{-1}\left[E_{jn}^{\pm\gamma}(z_\pm) - E_{jn}^{\pm(0)}(z_\pm)\right]\mathrm{e}^{\mathrm{i}(\alpha_n\cdot\rho\mp\beta_n^\pm z_\pm)}$$
$$= \sum_{|\alpha_n|\leqslant\omega_\pm} C_{jn}^{-1}E_{jn}^{\pm\gamma}(z_\pm)\mathrm{e}^{\mathrm{i}(\alpha_n\cdot\rho\mp\beta_n^\pm z_\pm)} - \sum_{|\alpha_n|\leqslant\omega_\pm} C_{jn}^{-1}E_{jn}^{\pm(0)}(z_\pm)\mathrm{e}^{\mathrm{i}(\alpha_n\cdot\rho\mp\beta_n^\pm z_\pm)}. \tag{4.6}$$

Substituting (4.4) into (4.6), we obtain an reconstructed grating surface function

$$\phi(\rho) \approx \sum_{|\alpha_n|\leqslant\omega_\pm} C_{jn}^{-1}E_{jn}^{\pm\gamma}(z_\pm)\mathrm{e}^{\mathrm{i}(\alpha_n\cdot\rho\mp\beta_n^\pm z_\pm)} - C_{j0}^{-1}\left(r + \mathrm{e}^{-2\mathrm{i}\kappa_+ z_+}\right)p_j$$

from the reflection configuration or

$$\phi(\rho) \approx \sum_{|\alpha_n|\leqslant\omega_\pm} C_{jn}^{-1}E_{jn}^{\pm\gamma}(z_\pm)\mathrm{e}^{\mathrm{i}(\alpha_n\cdot\rho\mp\beta_n^\pm z_\pm)} - C_{j0}^{-1}tp_j$$

from the transmission configuration.

Hence, only two fast Fourier transforms are needed to reconstruct the grating surface function: one is done for the data to obtain $E_{jn}^{\pm\gamma}(z_\pm)$ and another is done to obtain the approximated function ϕ.

5. Numerical experiment

In this section, we discuss the algorithmic implementation for the direct and inverse problems and present three numerical examples to illustrate the effectiveness of the proposed method. As is shown in figure 2, three types of grating profiles are considered. The first one is a smooth function with finitely many Fourier modes; the second one is a continuous but non-differentiable function; the third one is a discontinuous function with infinitely many Fourier modes. We comment that the proposed method is applicable to non-smooth functions numerically, although it requires smooth profiles $\psi \in C^2(\mathbb{R}^2)$ theoretically.

The second-order Nédélec edge element is adopted to solve the direct problem and obtain the synthetic scattering data. Uniaxial perfect matched layer (PML) boundary condition is imposed on the z direction to truncated the domain. An adaptive mesh refinement technique [20] is used to achieve the solution with a specified accuracy in an optimal fashion. Our implementation is based on parallel hierarchical grid (PHG) [51], which is a toolbox for developing parallel adaptive finite element programs on unstructured tetrahedral meshes. To have a tetrahedral mesh with biperiodic boundary points, we generate an uniform hexahedral mesh and then divide each hexahedron into six tetrahedrons. The linear system resulted from finite element discretization is solve by the multifrontal massively parallel sparse direct solver [1].

In the following three examples, the incident wave is taken as $\mathbf{E}^{\mathrm{inc}} = (1,0,0)\mathrm{e}^{-\mathrm{i}\kappa_+ z}$, i.e. $p_1 = 1$ and $p_2 = p_3 = 0$, and only the first component of the electric field, $E_1^+(\rho,h)$, needs to be measured. The wavenumber in Ω_S^- is $\kappa_- = 1.6\pi$. The wavenumber in Ω_S^+ is $\kappa_+ = \pi$, which corresponds to the wavelength $\lambda = 2$. Define by R the unit rectangular domain, i.e. $R = [0, 0.5\lambda] \times [0, 0.5\lambda]$. The computational domain is $R \times [-0.3\lambda, 0.3\lambda]$ with the PML region $(R \times [-0.3\lambda, -0.15\lambda]) \cup (R \times [0.15\lambda, 0.3\lambda])$. The scattering data $E_1^+(\rho,h)$ is obtained by interpolation into the uniform 256×256 grid points on the measurement plane $z = h$. In all the figures, the plots are rescaled with respect to the wavelength λ to clearly show the relative size. The results are plotted on 64×64 grid points instead of 256×256 grid points in order to reduce the display sizes. To test the stability of the method, a random noise is added to the scattering data, i.e. the scattering data takes the form

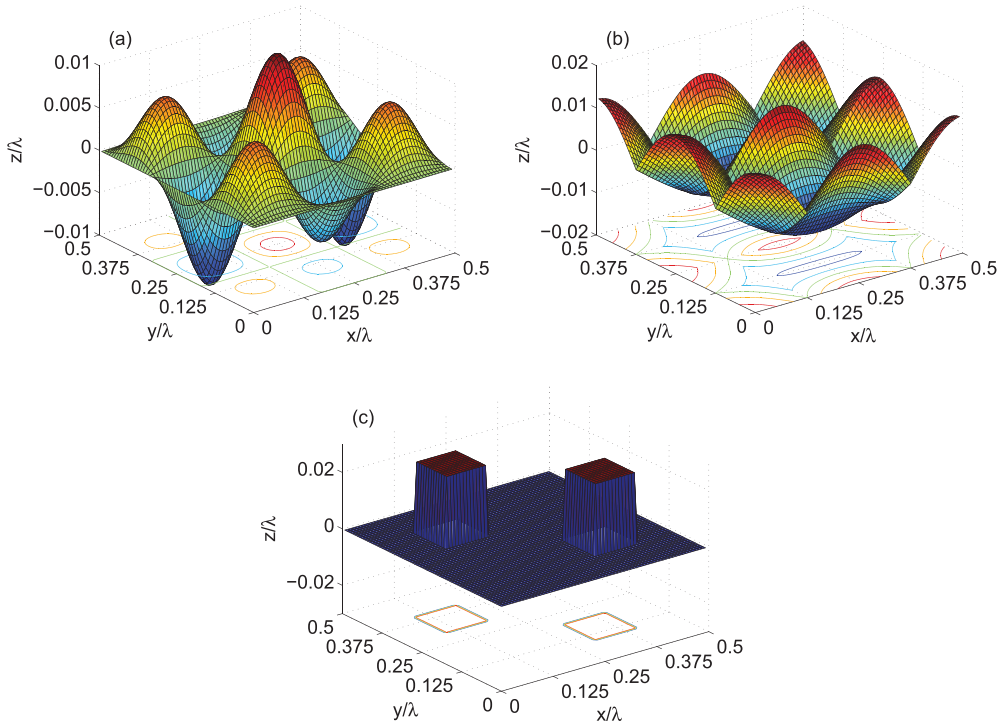

Figure 2. The exact grating profile ψ. (a) Example 1: a smooth grating profile with finitely many Fourier modes; (b) example 2: a continuous but non-differentiable grating profile; (c) example 3: a discontinuous grating profile.

$$E_1^{+\gamma}(\rho, h) = E_1^{+}(\rho, h)(1 + \gamma\,\mathrm{rand}),$$

where rand stands for uniformly distributed random numbers in $[-1,1]$ and γ is the noise level parameter. The relative $L^2(R)$ error is defined by

$$e = \frac{\|\phi - \phi_{\gamma,\delta}\|_{0,R}}{\|\phi\|_{0,R}},$$

where ϕ is the exact surface function and $\phi_{\gamma,\delta}$ is the reconstructed surface function.

Example 1. This example illustrates the reconstruction results of a smooth grating profile with finitely many Fourier modes, as seen in figure 2(a). The exact grating surface function is given by $\phi(\rho) = \delta\psi(\rho)$, where the grating profile function

$$\psi(x, y) = 0.5\sin(3\pi x)(\cos(2\pi y) - \cos(4\pi y)).$$

First, consider the surface deviation parameter δ. The measurement is taken at $h = 0.1\lambda$ and no additional random noise is added to the scattering data, i.e. $\gamma = 0$. This test is to investigate the influence of surface deformation parameter on the reconstructions. In (4.2), higher order terms of δ are dropped in the power series to linearize the inverse problem and to obtain the explicit reconstruction formulas. As expected, the smaller the surface deformation δ is, the more accurate is the approximation of the linearized model to the original nonlinear model problem. Table 1 shows the relative $L^2(R)$ error of the reconstructions with three different

Table 1. Example 1: relative error of the reconstructions by using different δ with $h = 0.1\lambda$ and $\gamma = 0.0$.

δ	0.05λ	0.025λ	0.0125λ
e	4.53×10^{-1}	2.49×10^{-1}	1.56×10^{-1}

Table 2. Example 1: relative error of the reconstructions by using different h with $\delta = 0.0125\lambda$ and $\gamma = 1\%$.

h	0.1λ	0.075λ	0.05λ	0.025λ
e	5.67×10^{-1}	2.95×10^{-1}	2.08×10^{-1}	1.67×10^{-1}

Table 3. Example 1: relative error of the reconstructions by using different h with $\delta = 0.0125\lambda$ and $\gamma = 5\%$.

h	0.1λ	0.075λ	0.05λ	0.025λ
e	8.38×10^{-1}	8.06×10^{-1}	5.56×10^{-1}	2.95×10^{-1}

surface deformation parameters $\delta = 0.05\lambda, 0.025\lambda, 0.0125\lambda$ for a fixed measurement distance $h = 0.1\lambda$. It is clear to note that the error decreases from 45.3% to 15.6% as δ decreases from 0.05λ to 0.0125λ.

Next is to consider the noise level γ and the measurement distance h. In practice, the scattering data always contains a certain amount of noise. To test the stability and super resolving capability of the method, we add 1% and 5% random noises to the scattering data. Tables 2 and 3 report the relative $L^2(R)$ error of the reconstructions with four different measurement distances $h = 0.1\lambda, 0.075\lambda, 0.05\lambda, 0.025\lambda$ for a fixed $\delta = 0.0125\lambda$. Comparing the results for the same $\delta = 0.0125\lambda$ and $h = 0.1\lambda$ in tables 1 and 3, we can see that the relative error increases dramatically from 15.6% by using noise free data to 83.8% by using 5% noise data. The reason is that a smaller cut-off should be chosen to suppress the exponentially increasing noise in the data and thus the Fourier modes of the exact grating surface function can not be recovered for those higher than the cut-off frequency, which leads to a large error and poor resolution in the reconstruction. A smaller measurement distance is desirable in order to have a large cut-off frequency, which enhances the resolution and reduces the error. As can be seen in table 2, the reconstruction error decreases from 56.7% by using $h = 0.1\lambda$ to as low as 16.7% by using $h = 0.025\lambda$ for 1% noise data. Similarly, in table 3, the reconstruction error decreases from 83.8% by using $h = 0.1\lambda$ to as low as 29.5% by using $h = 0.025\lambda$ even for 5% noise data. Figure 3 plots the reconstructed surfaces by using $h = 0.1\lambda, 0.075\lambda, 0.05\lambda, 0.025\lambda$. Comparing the exact surface profile in figure 2(a) and the reconstructed surface in figure 3(d), we can see that the reconstruction is almost perfect and the difference is little by carefully checking the contour plots.

Example 2. This example illustrates the reconstruction results of a continuous but non-differentiable grating profile with infinitely many Fourier modes, as seen in figure 2(b). The exact grating surface function is given by $\phi(\rho) = \delta\psi(\rho)$, where the grating profile function

$$\psi(x, y) = |\cos(2\pi x)\cos(2\pi y)| - |\sin(\pi x)\sin(2\pi y)|.$$

First is to consider the influence of δ by using noise-free data. The measurement is taken at $h = 0.1\lambda$. Table 4 presents the relative $L^2(R)$ error of the reconstructions with three different surface deformation parameters $\delta = 0.05\lambda, 0.025\lambda, 0.0125\lambda$. The error decreases from 35.8%

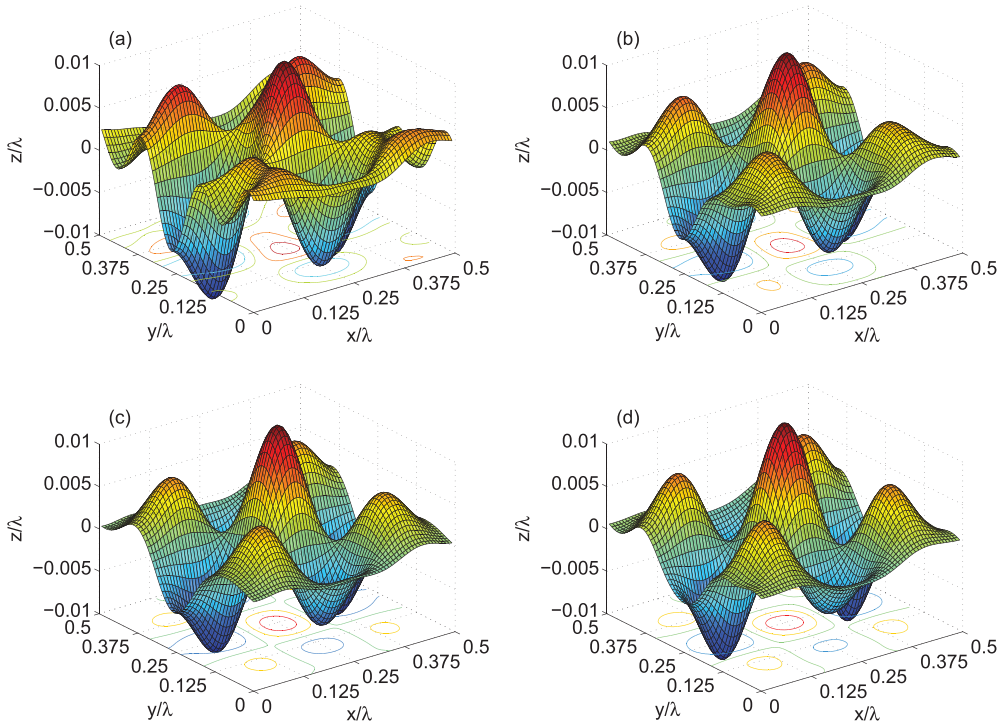

Figure 3. Example 1: reconstructed grating surfaces by using different h with $\delta = 0.0125\lambda$ and $\gamma = 1\%$. (a) $h = 0.1\lambda$; (b) $h = 0.075\lambda$; (c) $h = 0.05\lambda$; (d) $h = 0.025\lambda$.

to 16.0% as δ decreases from 0.05λ to 0.0125λ. Based on these results, the following observation can be made: a smaller deformation parameter δ yields a better reconstruction.

Next is to consider the influence of the noise level γ and the measurement distance h. We add 1% and 5% random noises to the scattering data. Tables 5 and 6 report the relative $L^2(R)$ error of the reconstructions with four different measurement distances $h = 0.1\lambda, 0.075\lambda, 0.05\lambda, 0.025\lambda$ for a fixed $\delta = 0.0125\lambda$. Comparing the results for the same $\delta = 0.0125\lambda$ and $h = 0.1\lambda$ in tables 4 and 6, we can see that the relative error is more than doubled from 16.0% by using noise-free data to 34.3% by using 5% noise data. Again, the reason is that a smaller cut-off is chosen to suppress the exponentially increasing noise in the data and thus higher Fourier modes of the exact grating surface function can not be recovered. A smaller measurement distance helps to enhance the resolution and reduce the error. In table 5, the reconstruction error decreases from 27.3% by using $h = 0.1\lambda$ to as low as 17.3% by using $h = 0.025\lambda$ for 1% noise data. In table 6, the reconstruction error decreases from 34.3% by using $h = 0.1\lambda$ to as low as 24.4% by using $h = 0.025\lambda$ for 5% noise data. Figure 4 shows the reconstructed surfaces by using $h = 0.1\lambda, 0.075\lambda, 0.05\lambda, 0.025\lambda$. Comparing the exact surface profile in figure 2(b) and the reconstructed surface in figure 4(d), we can see that a good reconstruction can still be obtained when using a small measurement distance.

Example 3. This example illustrates the reconstruction results of a discontinuous grating profile of infinitely many Fourier modes with slower decay rate, as seen in figure 2(c). The exact grating surface function is given by $\phi(\rho) = \delta\psi(\rho)$, where the grating profile function

Table 4. Example 2: relative error of the reconstructions by using different δ with $h = 0.1\lambda$ and $\gamma = 0.0$.

δ	0.05λ	0.025λ	0.0125λ
e	3.58×10^{-1}	2.72×10^{-1}	1.60×10^{-1}

Table 5. Example 2: relative error of the reconstructions by using different h with $\delta = 0.0125\lambda$ and $\gamma = 1\%$.

h	0.1λ	0.075λ	0.05λ	0.025λ
e	2.73×10^{-1}	2.44×10^{-1}	1.88×10^{-1}	1.73×10^{-1}

Table 6. Example 2: relative error of the reconstructions by using different h with $\delta = 0.0125\lambda$ and $\gamma = 5\%$.

h	0.1λ	0.075λ	0.05λ	0.025λ
e	3.43×10^{-1}	2.99×10^{-1}	2.81×10^{-1}	2.44×10^{-1}

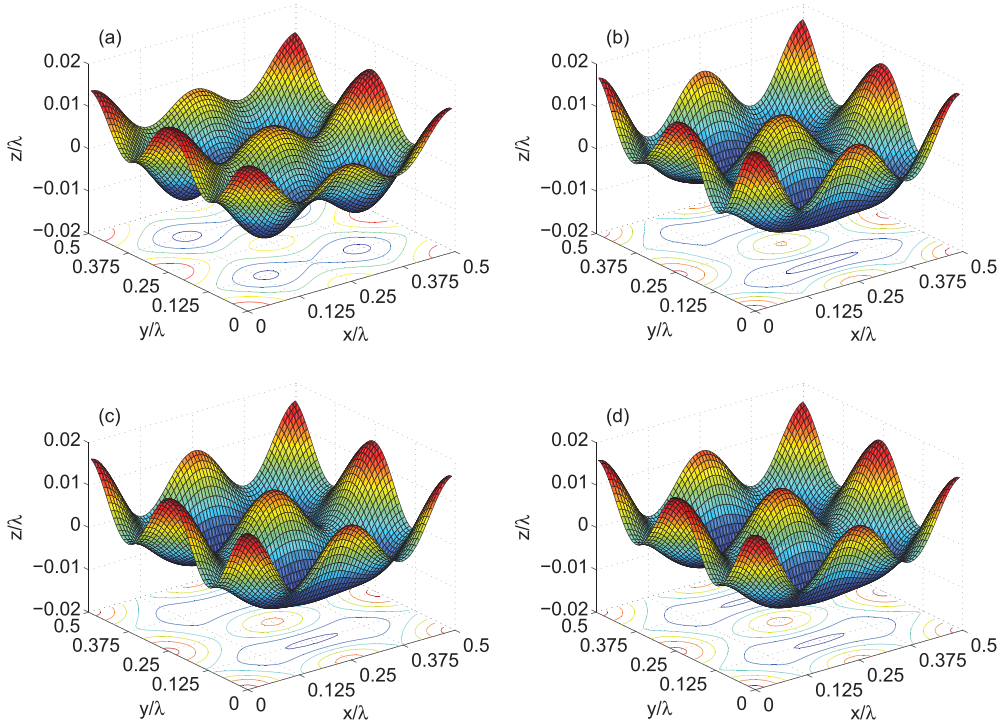

Figure 4. Example 2: reconstructed grating surfaces by using different h with $\delta = 0.0125\lambda$ and $\gamma = 1\%$. (a) $h = 0.1\lambda$; (b) $h = 0.075\lambda$; (c) $h = 0.05\lambda$; (d) $h = 0.025\lambda$.

Table 7. Example 3: relative error of the reconstructions by using different δ with $h = 0.1\lambda$ and $\gamma = 0.0$.

δ	0.05λ	0.025λ	0.0125λ
e	9.52×10^{-1}	7.80×10^{-1}	5.97×10^{-1}

Table 8. Example 3: relative error of the reconstructions by using different h with $\delta = 0.0125\lambda$ and $\gamma = 1\%$.

h	0.1λ	0.075λ	0.05λ	0.025λ
e	7.57×10^{-1}	7.25×10^{-1}	6.57×10^{-1}	5.94×10^{-1}

Table 9. Example 3: relative error of the reconstructions by using different h with $\delta = 0.0125\lambda$ and $\gamma = 5\%$.

h	0.1λ	0.075λ	0.05λ	0.025λ
e	8.51×10^{-1}	8.20×10^{-1}	7.90×10^{-1}	7.22×10^{-1}

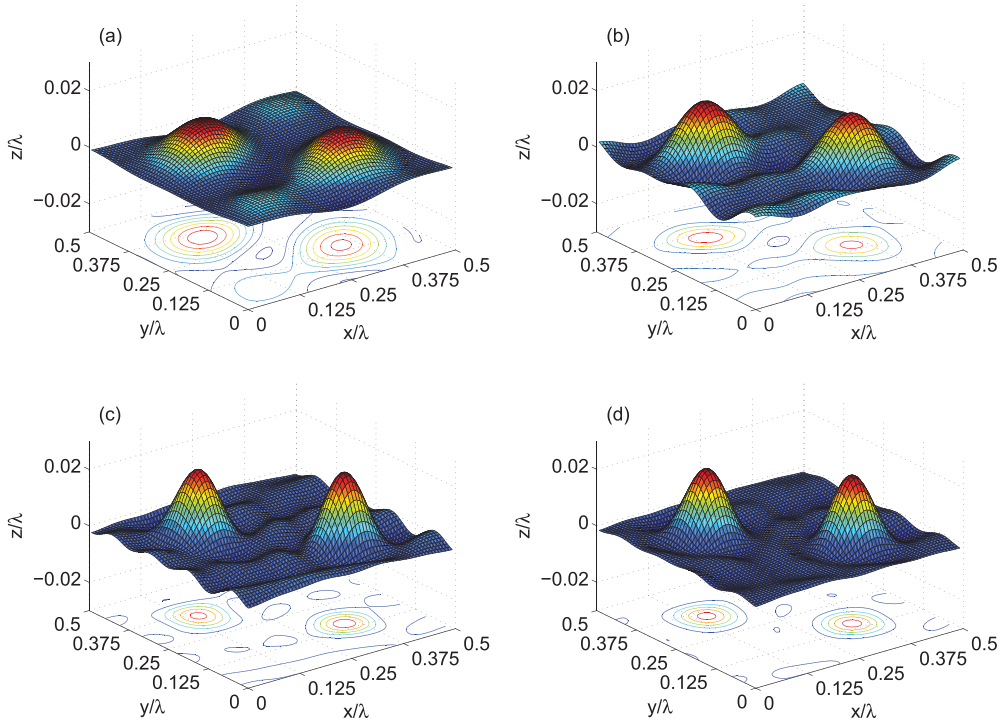

Figure 5. Example 3: reconstructed grating surfaces by using different h with $\delta = 0.0125\lambda$ and $\gamma = 1\%$. (a) $h = 0.1\lambda$; (b) $h = 0.075\lambda$; (c) $h = 0.05\lambda$; (d) $h = 0.025\lambda$.

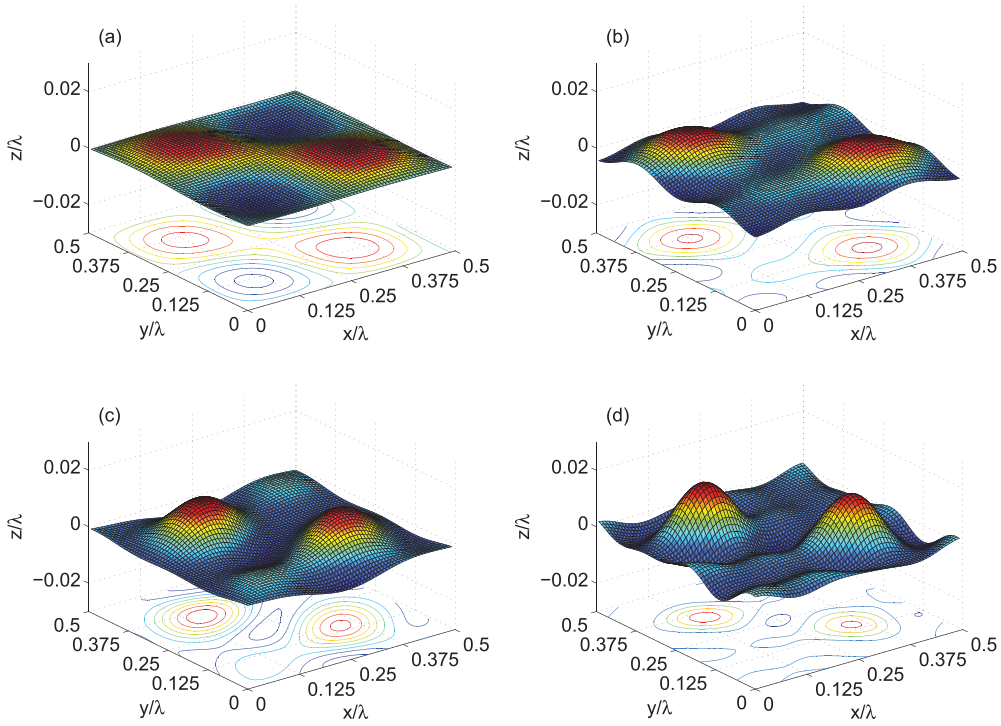

Figure 6. Example 3: reconstructed grating surfaces by using different h with $\delta = 0.0125\lambda$ and $\gamma = 5\%$. (a) $h = 0.1\lambda$; (b) $h = 0.075\lambda$; (c) $h = 0.05\lambda$; (d) $h = 0.025\lambda$.

$$\psi(x, y) = \chi_{[0.2,0.4]\times[0.6,0.8]} + \chi_{[0.6,0.8]\times[0.2,0.4]}.$$

Here χ is the characteristic function. This example reports the results for the binary grating.

First is to consider the influence of δ by using noise-free data. The measurement is taken at $h = 0.1\lambda$. Table 7 presents the relative $L^2(R)$ error of the reconstructions with three different surface deformation parameters $\delta = 0.05\lambda, 0.025\lambda, 0.0125\lambda$. The error decreases from 95.2% to 59.7% as δ decreases from 0.05λ to 0.0125λ. clearly, it shows that a smaller deformation parameter δ can yield a better reconstruction.

Next is to consider the influence of the noise level γ and the measurement distance h in order to investigate the stability and resolution. Again, we add 1% and 5% random noises to the scattering data. Tables 8 and 9 report the relative $L^2(R)$ error of the reconstructions with four different measurement distances $h = 0.1\lambda, 0.075\lambda, 0.05\lambda, 0.025\lambda$ for a fixed $\delta = 0.0125\lambda$. Comparing the results for the same $\delta = 0.0125\lambda$ and $h = 0.1\lambda$ in tables 7 and 9, we can see that the relative error is increased from 59.7% by using noise-free data to 85.1% by using 5% noise data. Again, the reason is that a smaller cut-off is chosen to suppress the exponentially increasing noise in the data and thus higher Fourier modes of the exact grating surface function can not be recovered. A smaller measurement distance helps to enhance the resolution and reduce the error. In table 8, the reconstruction error decreases from 75.7% by using $h = 0.1\lambda$ to as low as 59.4% by using $h = 0.025\lambda$ for 1% noise data. In table 9, the reconstruction error decreases from 85.1% by using $h = 0.1\lambda$ to as low as 72.2% by using $h = 0.025\lambda$ for 5% noise data. Figure 5 shows the reconstructed surfaces by using $h = 0.1\lambda, 0.075\lambda, 0.05\lambda, 0.025\lambda$.

Comparing the exact surface profile in figure 2(c) and the reconstructed surface in figure 5(d), we can see that a good reconstruction can still be obtained when using a small measurement distance even for such a binary grating.

6. Conclusion

We have presented an effective computational method to reconstruct surfaces of biperiodic dielectric gratings. Subwavelength resolution is achieved stably. Based on the transformed field expansion, an analytic solution is deduced for the direct problem. The nonlinear inverse problem is linearized by dropping higher order terms in power series. Explicit reconstruction formulas are obtained and are implemented by using the FFT. Three representative numerical examples are considered: one smooth function with finitely many Fourier modes and two non-smooth functions with infinitely many Fourier modes. We have carefully investigated the influence of the parameters on the reconstructions. The results show that super resolution may be achieved by using small measurement distance. There are many interesting and challenging mathematical problems, such as uniqueness, stability, resolution, and error estimates, which are remaining and left for future work. We will report the results elsewhere.

Acknowledgments

The research of XJ was supported in part by the China NSF grant 11401040 and by the Fundamental Research Funds for the Central Universities 24820152015RC17. The research of PL was partially supported by NSF DMS-1151308.

References

[1] Amestoy P R, Duff I S, Koster J and L'Excellent J-Y 2001 A fully asynchronous multifrontal solver using distributed dynamic scheduling *SIAM. J. Matrix Anal. Appl.* **23** 15–41
[2] Ammari H 1995 Uniqueness theorems for an inverse problem in a doubly periodic structure *Inverse Problems* **11** 823–33
[3] Ammari H and Bao G 2003 Maxwell's equations in periodic chiral structures *Math. Nachr.* **251** 3–18
[4] Ammari H, Garnier J and Solna K 2013 Resolution and stability analysis in full-aperture, linearized conductivity and wave imaging *Proc. Am. Math. Soc.* **141** 3431–46
[5] Ammari H, Kang H, Lim M and Zribi H 2010 Conductivity interface problems I. Small perturbation of an interface *Trans. Am. Math. Soc.* **362** 2435–49
[6] Ammari H and Zhang H 2015 A mathematical theory of super-resolution by using a system of sub-wavelength Helmholtz resonators *Commun. Math. Phys.* **337** 379–428
[7] Ammari H and Zhang H 2015 Super-resolution in high-contrast media *Proc. R. Soc.* A **471** 20140946
[8] Akduman I, Kress R and Yapar A 2006 Iterative reconstruction of dielectric rough surface profiles at fixed frequency *Inverse Problems* **22** 939–54
[9] Arens T and Kirsch A 2003 The factorization method in inverse scattering from periodic structures *Inverse Problems* **19** 1195–211
[10] Bao G 1994 A unique theorem for an inverse problem in periodic diffractive optics *Inverse Problems* **10** 335–40
[11] Bao G 1997 Variational approximation of Maxwell's equations in biperiodic structures *SIAM J. Appl. Math.* **57** 364–81
[12] Bao G, Cowsar L and Masters W 2001 *Mathematical Modeling in Optical Science: Volume 22 of Frontiers in Applied Mathematics* (Philadelpia, PA: SIAM)
[13] Bao G, Cui T and Li P 2014 Inverse diffraction grating of Maxwell's equations in biperiodic structures *Opt. Express* **22** 4799–816

[14] Bao G, Dobson D and Cox J A 1995 Mathematical studies in rigorous grating theory *J. Opt. Soc. Am.* A **12** 1029–42
[15] Bao G and Friedman A 1995 Inverse problems for scattering by periodic structure *Arch. Rational Mech. Anal.* **132** 49–72
[16] Bao G and Li P 2013 Near-field imaging of infinite rough surfaces *SIAM J. Appl. Math.* **73** 2162–87
[17] Bao G and Li P 2014 Near-field imaging of infinite rough surfaces in dielectric media *SIAM J. Imaging Sci.* **7** 867–99
[18] Bao G and Li P 2014 Convergence analysis in near-field imaging *Inverse Problems* **30** 085008
[19] Bao G and Lin J 2013 Near-field imaging of the surface displacement on an infinite ground plane *Inverse Problem Imag.* **7** 377–96
[20] Bao G, Li P and Wu H 2009 An adaptive edge element method with perfectly matched absorbing layers for wave scattering by biperiodic structures *Math. Comput.* **79** 1–34
[21] Bao G, Li P and Wu H 2012 A computational inverse diffraction grating problem *J. Opt. Soc. Am.* A **29** 394–9
[22] Bao G, Li P and Lv J 2013 Numerical solution of an inverse diffraction grating problem from phaseless data *J. Opt. Soc. Am.* A **30** 293–9
[23] Bao G, Zhang H and Zou J 2011 Unique determination of periodic polyhedral structures by scattered electromagnetic fields *Trans. Am. Math. Soc.* **363** 4527–51
[24] Bao G and Zhou Z 1998 An inverse problem for scattering by a doubly periodic structure *Trans. Am. Math. Soc.* **350** 4089–103
[25] Bruckner G, Cheng J and Yamamoto M 2002 An inverse problem in diffractive optics: conditional stability *Inverse Problems* **18** 415–33
[26] Bruckner G and Elschner J 2003 A two-step algorithm for the reconstruction of perfectly reflecting periodic profiles *Inverse Problems* **19** 315–29
[27] Bruno O and Reitich F 1993 Numerical solution of diffraction problems: a method of variation of boundaries *J. Opt. Soc. Am.* A **10** 1168–75
[28] Carney S and Schotland J 2000 Inverse scattering for near-field microscopy *Appl. Phys. Lett.* **77** 2798–800
[29] Carney S and Schotland J 2003 Near-field tomography *MSRI Ser. Math. Appl.* **47** 133–68
[30] Cheng T, Li P and Wang Y 2013 Near-field imaging of perfectly conducting grating surfaces *J. Opt. Soc. Am.* A **30** 2473–81
[31] Coifman R, Goldberg M, Hrycak T, Israeli M and Rokhlin V 1999 An improved operator expansion algorithm for direct and inverse scattering computations *Waves Random Media* **9** 441–57
[32] Courjon D 2003 *Near-Field Microscopy and Near-Field Optics* (London: Imperial College Press)
[33] Courjon D and Bainier C 1994 Near field microscopy and near field optics *Rep. Prog. Phys.* **57** 989–1028
[34] DeSanto J A and Wombell R J 1991 The reconstruction of shallow rough-surface profiles from scattered field data *Inverse Problems* **7** L7–12
[35] Dobson D 1994 A variational method for electromagnetic diffraction in biperiodic structures *Math. Modelling Numer. Anal.* **28** 419–39
[36] Elschner J, Hsiao G and Rathsfeld A 2003 Grating profile reconstruction based on finite elements and optimization techniques *SIAM J. Appl. Math.* **64** 525–45
[37] Giard C and Dereux A 1996 Near-field optics theories *Rep. Prog. Phys.* **59** 657–99
[38] Hettlich F 2002 Iterative regularization schemes in inverse scattering by periodic structures *Inverse Problems* **18** 701–14
[39] Hettlich F and Kirsch A 1997 Schiffer's theorem in inverse scattering theory for periodic structures *Inverse Problems* **13** 351–61
[40] Hu G, Yang J and Zhang B 2011 An inverse electromagnetic scattering problem for a bi-periodic inhomogeneous layer on a perfectly conducting plate *Appl. Anal.* **90** 317–33
[41] Hu G and Zhang B 2011 The linear sampling method for inverse electromagnetic scattering by a partially coated bi-periodic structures *Math. Methods Appl. Sci.* **34** 509–19
[42] Ito K and Reitich F 1999 A high-order perturbation approach to profile reconstruction: I. Perfectly conducting gratings *Inverse Problems* **15** 1067–85
[43] Kirsch A 1994 Uniqueness theorems in inverse scattering theory for periodic structures *Inverse Problems* **10** 145–52
[44] Kress R and Tran T 2000 Inverse scattering for a locally perturbed half-plane *Inverse Problems* **16** 1541–59
[45] Lechleiter A and Nguyen D L 2013 On uniqueness in electromagnetic scattering from biperiodic structures *ESAIM: M2AN* **47** 1167–84

[46] Lechleiter A and Nguyen D L 2013 Factorization method for electromagnetic inverse scattering from biperiodic structures *SIAM J. Imaging Sci.* **6** 1111–39
[47] Malcolm A and Nicholls D P 2011 A boundary perturbation method for recovering interface shapes in layered media *Inverse Problems* **27** 095009
[48] Nédélec J C and Starling F 1991 Integral equation methods in a quasi-periodic diffraction problem for the time-harmonic Maxwell's equations *SIAM J. Math. Anal.* **22** 1679–701
[49] Nicholls D P and Reitich F 2004 Shape deformations in rough surface scattering: cancellations, conditioning, and convergence *J. Opt. Soc. Am.* A **21** 590–605
[50] Petit R (ed) 1980 *Electromagnetic Theory of Gratings* (Berlin: Springer)
[51] PHG (Parallel Hierarchical Grid) http://lsec.cc.ac.cn/phg/
[52] Yang J and Zhang B 2011 Inverse electromagnetic scattering problems by a doubly periodic structure *Math. Appl. Anal.* **18** 111–26